TRANSITION CHARACTERISTICS OF A VTOL AIRCRAFT POWERED BY FOUR DUCTED TANDEM PROPELLERS

by Edwin E. Davenport and Kenneth P. Spreemann

Langley Research Center
Langley Station, Hampton, Va.

TRANSITION CHARACTERISTICS OF A VTOL AIRCRAFT

POWERED BY FOUR DUCTED TANDEM PROPELLERS

By Edwin E. Davenport and Kenneth P. Spreemann

Langley Research Center
Langley Station, Hampton, Va.

NATIONAL AERONAUTICS AND SPACE ADMINISTRATION

TRANSITION CHARACTERISTICS OF A VTOL AIRCRAFT

POWERED BY FOUR DUCTED TANDEM PROPELLERS

By Edwin E. Davenport and Kenneth P. Spreemann
Langley Research Center

SUMMARY

Results are presented of a wind-tunnel investigation of the aerodynamic stability and control characteristics of a vertical take-off and landing (VTOL) aircraft configuration powered by four tilting ducted propellers arranged in tandem pairs. The two front ducted propellers were mounted close inboard and near the top of the fuselage on the same level as the rear ducted propellers which were mounted outboard on the tips of a short wing.

The results indicate that the nose-up moment encountered in transition arises from two sources: the nose-up moment of the ducts themselves and the downwash at the rear element (pair of ducts and wing) which reduces the percentage of the lift produced by the rear element.

The use of differential duct incidence alone or differential thrust alone as a means of achieving trim in transition requires relatively large increments of either for trim. A more practical solution may be the use of both differential incidence and thrust with some differential incidence being used for trim and differential thrust reserved mainly for longitudinal control.

INTRODUCTION

Ducted propellers continue to be of interest for vertical take-off and landing (VTOL) aircraft because the duct prevents contraction of the slipstream and reduces the tip losses encountered by an unducted propeller, with an attendant reduction in the diameter required to achieve a specific thrust. The more compact aircraft made possible by the use of ducted propellers coupled with the protection afforded by the ducts makes the ducted-propeller configuration attractive for carrier applications.

By arranging four ducted propellers in tandem pairs (as pointed out in ref. 1) excellent pitch and roll control can be obtained in hovering by means of differential thrust of appropriate pairs of ducted propellers. Ducted propellers, however, experience a larger nose-up moment in transition from hovering to forward flight than would occur on unshrouded propellers. The tandem arrangement provides two possible means of trimming these moments: differential thrust and differential incidence of the front and rear pairs.

The present investigation was undertaken as part of a program to study the transition characteristics of a dual tandem ducted-propeller configuration and specifically to study the effectiveness of differential thrust and differential incidence of the front and rear ducted propellers in producing trim and control in transition. The model was specially instrumented so that the forces and moments carried on the front pair of ducts and on the rear element (pair of ducts and wing) could be measured separately to aid in analyzing the characteristics in transition.

This investigation is an extension of the work presented in reference 2. Some preliminary results of the present study were incorporated in reference 3.

SYMBOLS

All forces and moments are referred to the stability-axis system, which is an orthogonal system, with the origin at the center of moments. The positive sense of forces, moments, and angles is shown in figure 1.

C_T thrust coefficient, $\dfrac{T}{\rho n^2 D^4}$

D inside diameter of ducts, 1.167 ft

F_X longitudinal force, lb

i_d incidence of duct thrust axis, relative to fuselage center line, deg

L lift of complete model, lb

L_F, L_R lift of front and rear duct assemblies (wing and duct), respectively, lb

L_X lift of either front or rear duct, lb

M pitching moment, ft-lb

g acceleration due to gravity, 32.2 ft/sec^2

N propeller rotational speed, rpm

n propeller rotational speed, rps

q free-stream dynamic pressure, lb/sq ft

ρ mass density of air in free stream, slugs/cu ft

T thrust of ducted propeller, lb (see fig. 1)

V_O airspeed, knots

2

V_t propeller tip speed, knots

x   distance between center of moments for complete model and center of
            moments for duct assembly balance, 26.60 in. (see fig. 2)

μ tip speed ratio, $\dfrac{V_o}{V_t}$

α angle of attack of fuselage center line, deg

Subscripts:

F   front

R   rear

MODEL

The model configuration, as shown in figure 2, consisted of a stubby box-like fuselage made of plywood with balsa wood fairings, with two front ducted propellers mounted close inboard and two rear ducted propellers mounted outboard on the tips of a short wing. The geometric characteristics of the model are given in table I. Both front and rear ducted assemblies were mounted near the top of the fuselage and were equipped with vanes, which for the present investigation were never deflected. This model was used in the investigation of reference 2. The fixed pitch propellers were tested statically and then set at blade angles that gave approximately the same thrust for each set of propellers. The propeller power was supplied by a-c induction motors wired in parallel sets to variable-frequency power control units. With this system the rotational speed of the front ducted propellers and rear ducted propellers could be varied independently.

The ducted-propeller pairs were mounted at the 50-percent-chord station of the ducts on the front and rear duct strain-gage balances so that the lift, drag, and pitching moment of the front and rear elements could be measured directly. The rear duct balance measured the loads carried on the rear wing and ducts. A third strain-gage balance was mounted at the moment reference point, shown in figure 2, to measure the complete model forces and moments.

Tuft-grid pictures depicting the flow at the plane of the rear duct were obtained by removing the rear duct and wing and placing the plane of the tuft grid at the 50-percent-chord station of the rear duct. The tuft grid was attached to the model support and moved with the model. A camera was mounted on the tunnel floor to the rear of the model. This arrangement permitted tuft-grid photographs to be taken throughout the angle-of-attack range. It should be noted here that the front duct assembly was mounted in a low position on the fuselage during the tuft-grid portion of the investigation.

Essentially, three groups of tests were made. The first group consisted of tests of the model through an angle-of-attack range at constant propeller rotational speed and rear duct incidence for various values of front duct incidence. The second group included differential thrust tests with variable front ducted-propeller rotational speed. For both the first and second group of tests the tunnel speed was established as that required for zero net longitudinal force at zero angle of attack. This condition corresponds to steady level flight at zero angle of attack. The tunnel dynamic pressures used in the tests are noted in the data figures. Accelerating and decelerating conditions were covered in the last group of tests, most of which were made with 15° differential incidence between the front and rear pairs of ducts and with the front and rear rotational-speed differential required for pitching-moment trim in the non-accelerating condition at zero angle of attack.

Angle of attack was varied from -10° to 25° (nominal settings). The true angle of attack, with allowance for support deflection, was measured at each data point with a pendulum-type pickup mounted inside the model. Duct incidence angle varied from 0° to 90° and was measured with an inclinometer after each test. Propeller rotational speed ranged from about 3,600 to 5,600 rpm and was measured with four-pole magnetic pickup tachometers which were read out on a stroboscopic-type instrument.

PRESENTATION OF RESULTS

In view of the fact that large forces and moments due to power are encountered even at low dynamic pressure, it was impractical to present the data in conventional coefficient form. It is, therefore, presented in terms of nondimensional ratios: $M/DL_{\alpha=10}$, $L/L_{\alpha=10}$, and $F_X/L_{\alpha=10}$ for both complete models and the front and rear sets of duct characteristics. The values of $L_{\alpha=10}$ used to nondimensionalize the data were always taken from the complete model balance. An outline of the contents of the data figures is as follows:

DISCUSSION

Flow Field at Rear Duct

The tuft-grid pictures shown in figure 3 give an indication of the flow field that exists at the rear duct. These photographs were taken with the front duct in a low position, whereas the force data were obtained with it in the high position. This difference would affect the carryover forces across the fuselage but would not be expected to alter the primary features of the flow at the rear element. The rear duct position has been indicated on the tuft-grid photographs in proper relationship to the front duct position.

It can be noted that at a front duct incidence of zero, the vortex from the front duct travels almost straight back from the outer edge of the front duct. At higher duct incidence angles the vortex moves outboard and down. At some of the low-speed high-power conditions, the tip vortex apparently goes below the tuft grid. The possible effects of the vortex entering the rear duct (as it does in some conditions (fig. 3(f)) on the structural dynamics of the system are not known.

Basic Configuration

The basic data (fig. 4) with equal incidence and equal thrust for both front and rear ducted propellers were obtained at the combinations of tunnel speed and model power required to give zero drag at zero angle of attack. These conditions correspond to a steady level flight transition at zero angle of attack. At higher angles of attack a drag force is shown, indicating deceleration or descending flight.

The expected nose-up moments were encountered as the duct angle was increased in transition (fig. 4(a)). Also, attitude instability (positive $dM/d\alpha$) is indicated at the higher duct angles and lower speeds. This instability is common to most VTOL configurations at low speeds and, as pointed out in reference 3 wherein these results were analyzed, is rather mild and probably would not be objectionable.

The transition characteristics of a hypothetical 15,000-pound airplane have been estimated from the model data by assuming that the model was a 1/6-scale model of the full-scale airplane. The nose-up moments for the hypothetical airplane in transition, shown in figure 19, were computed from the data of figure 4. The maximum nose-up moment occurs at about 40 knots at 60° duct incidence and is equal to the weight of the airplane with a moment arm equal to 60 percent of the duct diameter.

As can be seen from the breakdown of forces and moments presented in figure 20, based on the data of figure 4, the problem of nose-up moment in transition arises from two sources: the direct nose-up moment of the ducts themselves and the difference in lift of the front and rear elements. At a duct incidence of 60°, where the out-of-trim moments are largest, the primary contribution is the difference in lift of the front and rear units. At this duct

angle, the rear element is carrying less than one-half of the lift (rear duct
element about 40 percent, front duct element about 54 percent, and fuselage
6 percent) due to the large downwash at the rear element (fig. 3(h)). The wing
between the rear ducts and the fuselage had a symmetrical airfoil section and
was set at zero incidence. The use of a cambered section and some incidence
may be helpful in reducing the nose-up moments in this region but the idea was
not investigated.

Differential Incidence

The effects of differential duct incidence are presented in figures 4 to 8
and a cross plot of the moments at 0° angle of attack is presented in fig-
ure 21(a). As can be seen from figure 21(a), at high duct incidence angles
(60° to 70°) differential incidence of the order of 30° to 40°, which may be
impractical, is required for trim. At lower incidence angles the use of dif-
ferential incidence for trim appears to be more practical.

Differential Thrust

The aerodynamic characteristics obtained with differential thrust are pre-
sented in figures 9 to 12 and the cross plot for the pitching moments at 0°
angle of attack is shown as figure 21(b). Inasmuch as the propeller thrusts
could not be measured directly on the model, as it was instrumented, the cross-
plotted data are presented as a function of the square of the propeller speed
ratio N_F/N_R which is approximately equal to the thrust ratio T_F/T_R, assuming
no change in propeller thrust coefficient C_T with n (at constant blade
angle). The data indicate that trim can be obtained by differential thrust
but the front thrust must drop to 50 to 60 percent of the rear thrust. If a
control moment in addition to trim was desired, it would become necessary to
further reduce the front thrust.

A possible compromise would be to use some differential incidence to
reduce the trim problem so that less differential thrust would be required for
the remainder of the trim and for control. The data of figures 13 to 18 were
obtained with 15° differential incidence and at combinations of tunnel speed
and model power to cover accelerating and decelerating flight conditions as well
as steady level flight transition. The differential propeller speed required
for pitch trim in steady level flight was used. The results shown in figure 22
indicate that while trimmed flight was achieved at 0° angle of attack for
steady level flight, fairly large out-of-trim moments are experienced in the
accelerating and decelerating conditions.

CONCLUDING REMARKS

From the results of a wind-tunnel investigation conducted to study the
aerodynamic characteristics of a four ducted-propeller tandem VTOL aircraft,
the following remarks apply:

The nose-up moment encountered in transition arises from two sources: the nose-up moment of the ducts themselves and the downwash at the rear element (pair of ducts and wing) which reduces the percentage of the lift produced by the rear element.

The use of differential duct incidence alone or differential thrust alone as a means of achieving trim in transition requires relatively large increments of either for trim. A more practical solution may be the use of both differential incidence and thrust with some differential incidence being used for trim and differential thrust reserved mainly for longitudinal control.

Langley Research Center,
    National Aeronautics and Space Administration,
        Langley Station, Hampton, Va., December 12, 1963.

REFERENCES

1. Paxhia, Vincent B., and Sing, Edward Y.: Design Development of a Dual Tandem Ducted Propeller VTOL Aircraft. Paper No. 63-30, Inst. Aerospace Sci., Jan. 1963.

2. Newsom, William A., Jr.: Aerodynamic Characteristics of Four-Duct Tandem VTOL-Aircraft Configurations. NASA TN D-1481, 1963.

3. McKinney, M. O., and Newsom, W. A.: Experimental Research on 4-Duct Tandem VTOL Aircraft Configurations. Presented at Eighteenth Annual Forum of American Helicopter Soc. (Washington, D.C.), May 3-5, 1962.

TABLE I.- GEOMETRIC CHARACTERISTICS OF MODEL

Body:
  Maximum height, in. 15.40
  Maximum width, in. 15.40
  Length, in. 86.00
  Distance of forward-duct pivot aft of nose, in. 11.00
  Distance between duct pivots, in. 53.20
  Distance of rear-duct pivot below top of fuselage, in. 2.40
  Distance of front-duct pivot below top of fuselage, in. 2.40

Wing:
  Span, in. 78.60
  Chord, in. 12.00
  Airfoil section . . . . NACA 0015

Ducts:
  Outside diameter, in. 17.25
  Inside diameter, in. 14.00
  Exit diameter, in. 15.96
  Length, in. 9.00
  Pivot point, percent duct chord 50.00
  Airfoil section (maximum camber facing inward) . . . . NACA 2418

Propeller diameter, in. 13.75
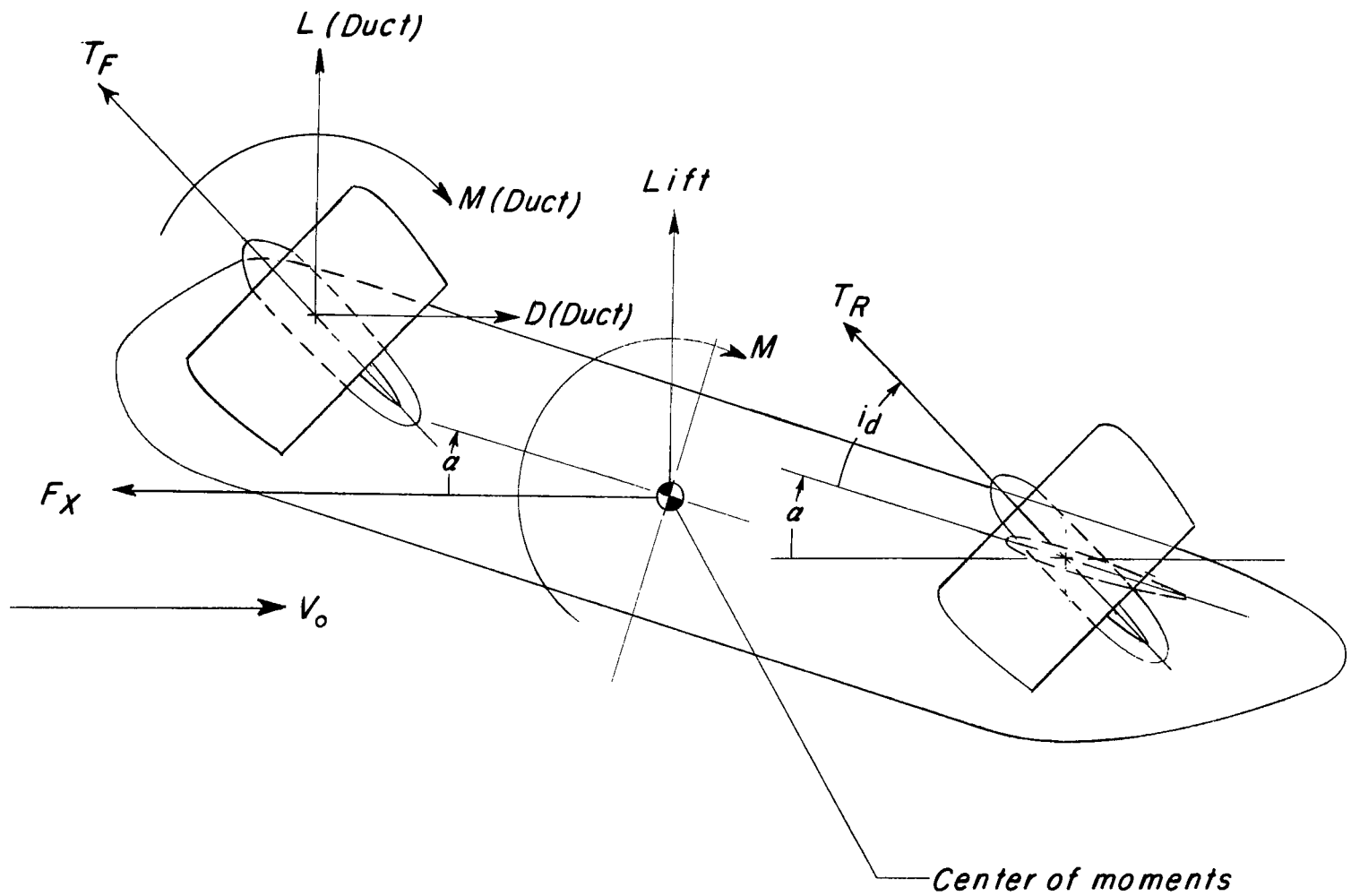
Figure 1.- Positive sense of forces, moments, and angles.

15.96

12.40

9.0

78.60

49.90

32.65

61.35

Center of moments

26.60 26.60

Duct pivot
on .50 chord
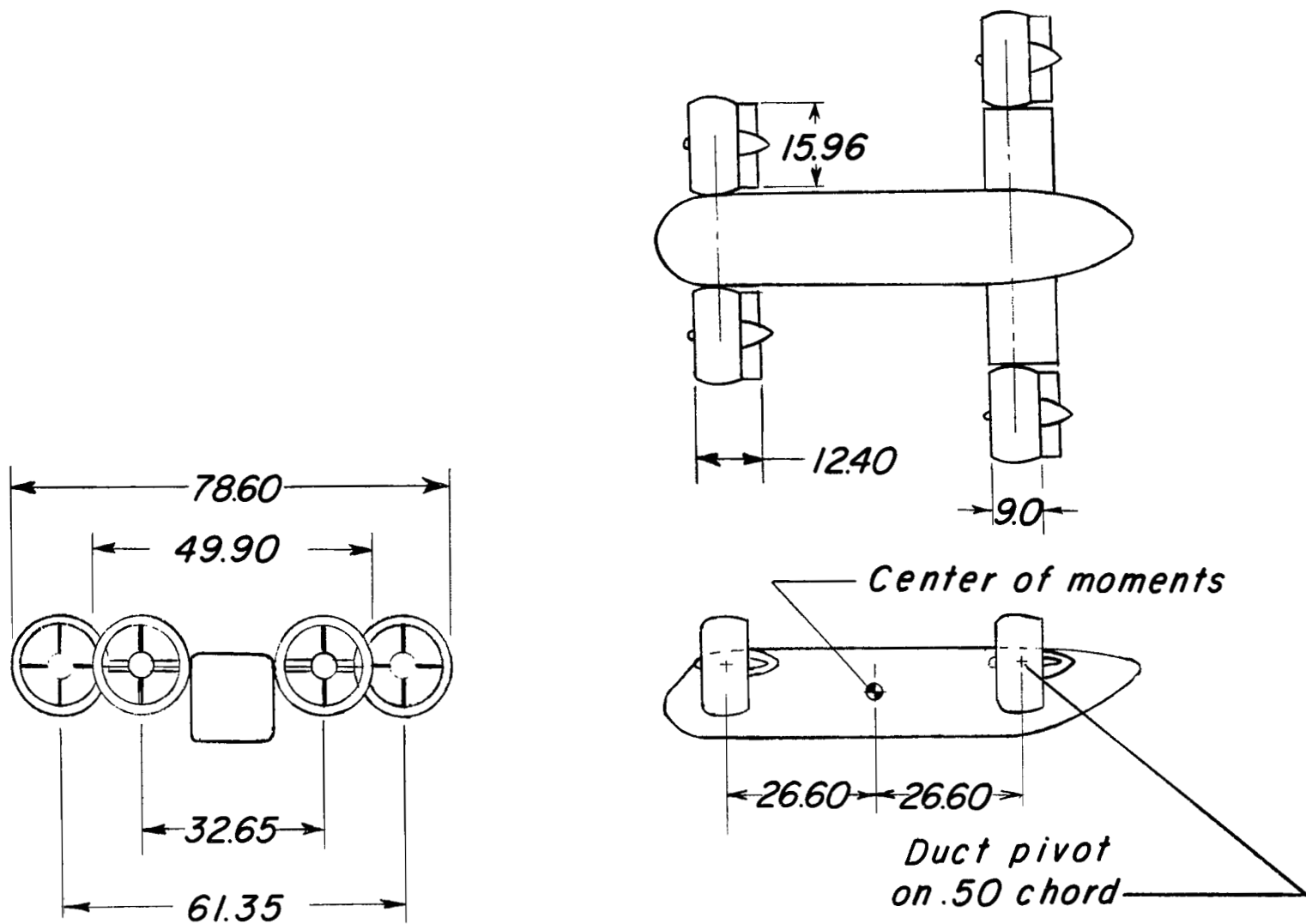
Figure 2.- Model dimensions. All dimensions are in inches.
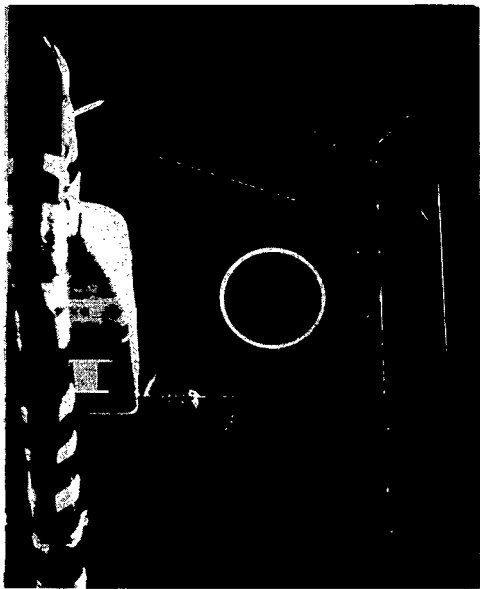
$\alpha = -10°$

$\alpha = 0°$
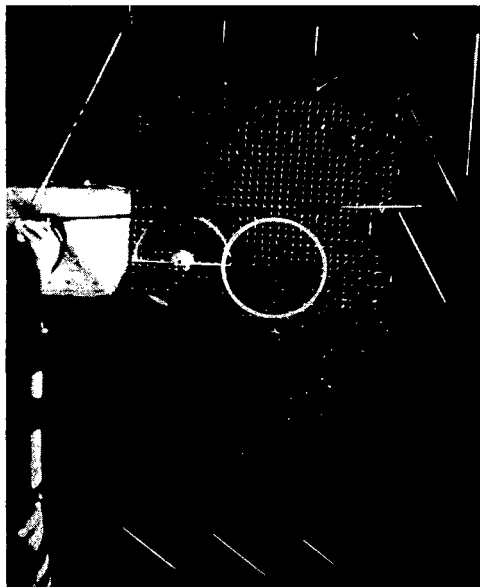
$\alpha = 10°$
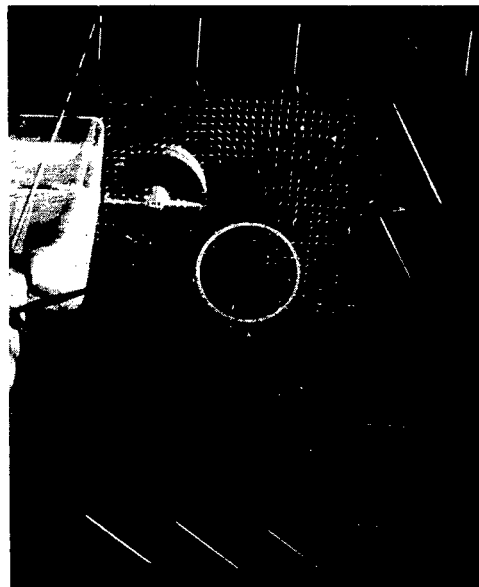
$\alpha = 20°$

(a) $i_d = 0°$; N = 4,976 rpm; q = 5.08; μ = 0.215.   L-63-9270
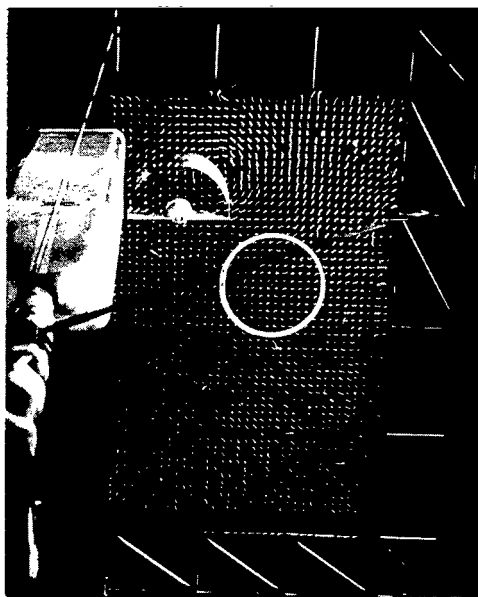
Figure 3.- Tuft grid at rear duct position.
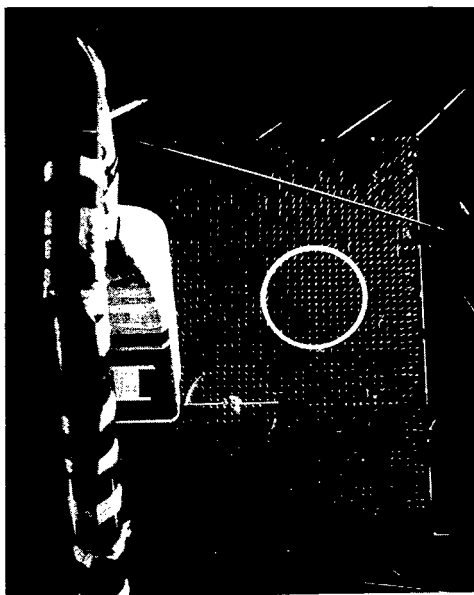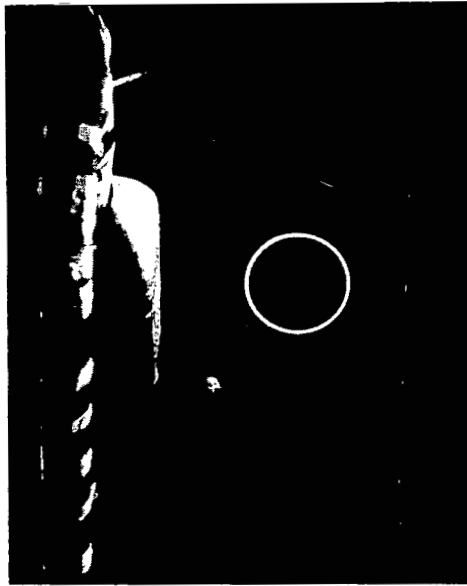
$$\alpha = -10°$$
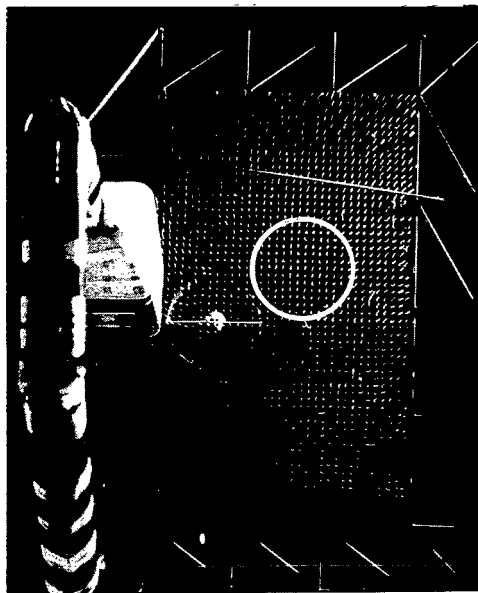
$$\alpha = 0°$$
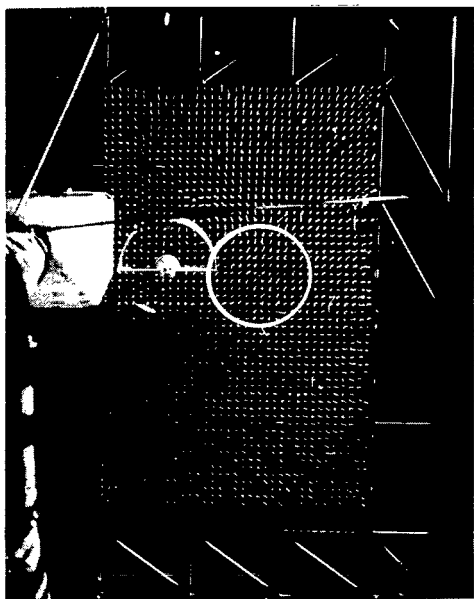
$$\alpha = 10°$$

$$\alpha = 20°$$

(b) $i_d = 0°$; N = 4,982 rpm; q = 3.88; μ = 0.188.

L-63-9271

Figure 3.- Continued.

$\alpha = -10°$
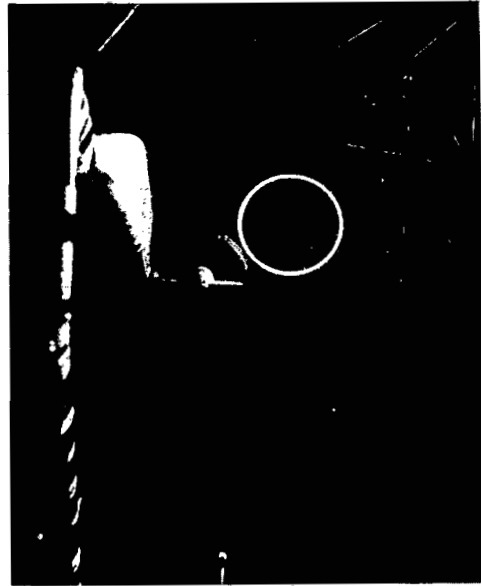
$\alpha = 0°$
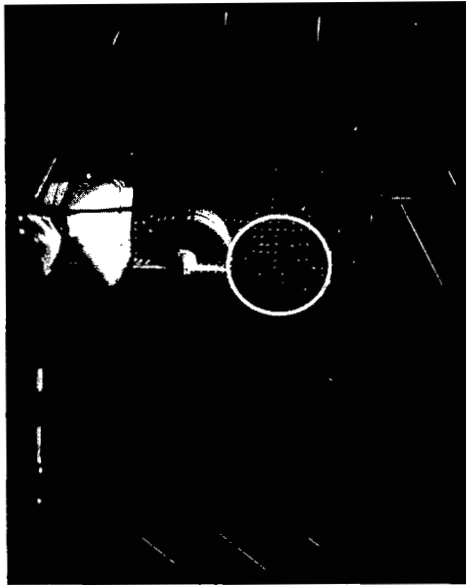
$\alpha = 10°$
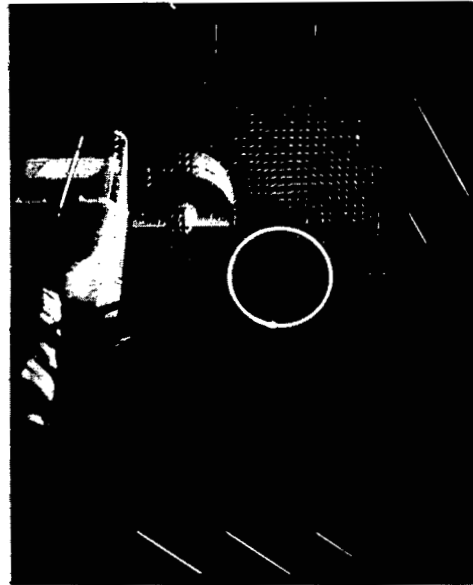
$\alpha = 20°$

(c) $i_d = 15°$; N = 3,936 rpm; q = 3.95; μ = 0.240.   L-63-9272

Figure 3.- Continued.
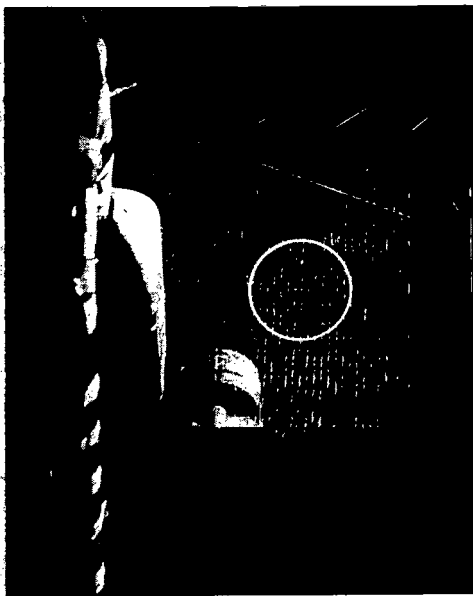
$\alpha = -10°$
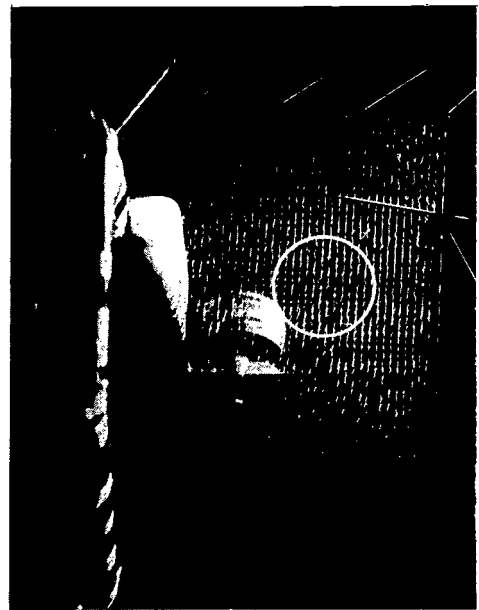
$\alpha = 0°$
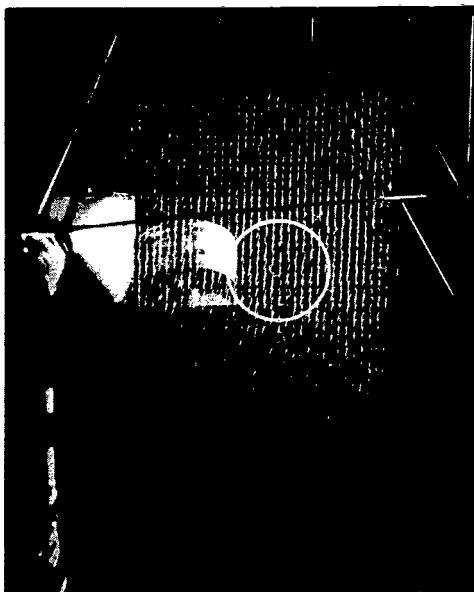
$\alpha = 10°$
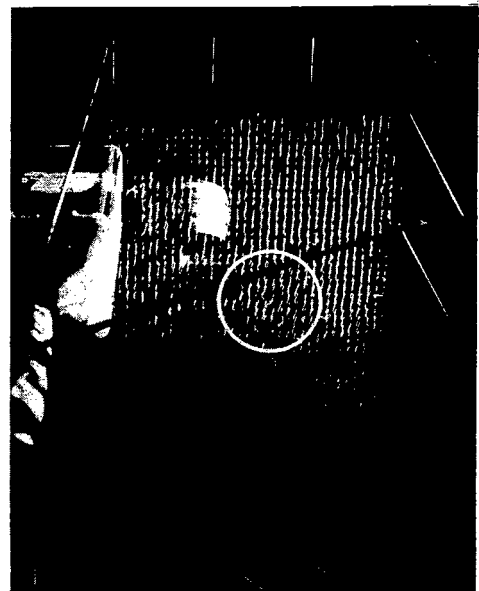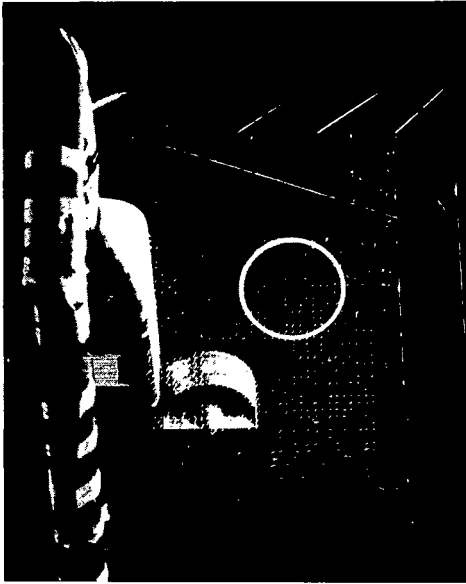
$\alpha = 20°$
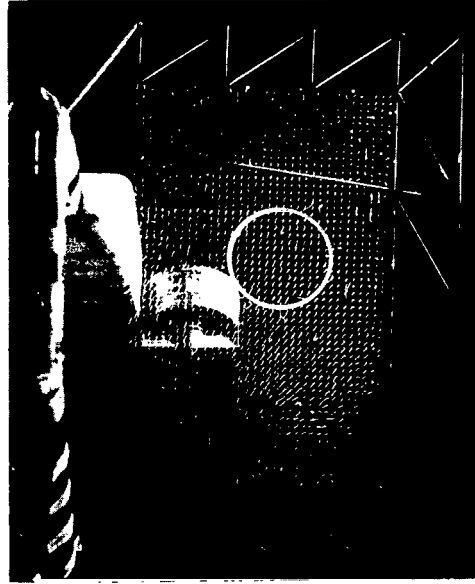
(d) $i_d = 44°$; N = 3,769 rpm; q = 0.12; $\mu = 0.044$.

L-63-9273

Figure 3.- Continued.

14

$\alpha = -10°$

$\alpha = 0°$
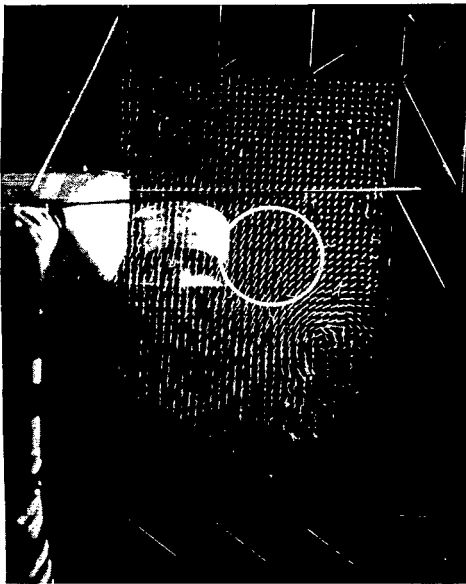
$\alpha = 10°$
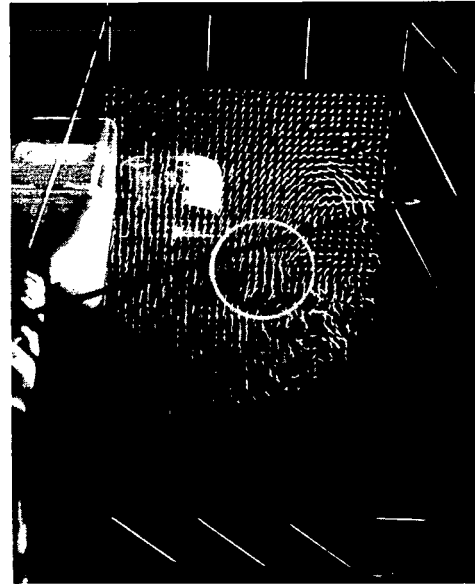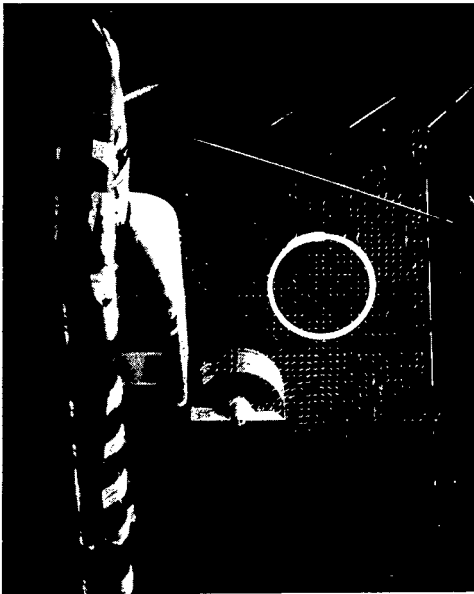
$\alpha = 20°$

(e) $i_d = 44°$; N = 3,666 rpm; q = 0.21; μ = 0.059.

L-63-9274

Figure 3.- Continued.

$$\alpha = -10°$$
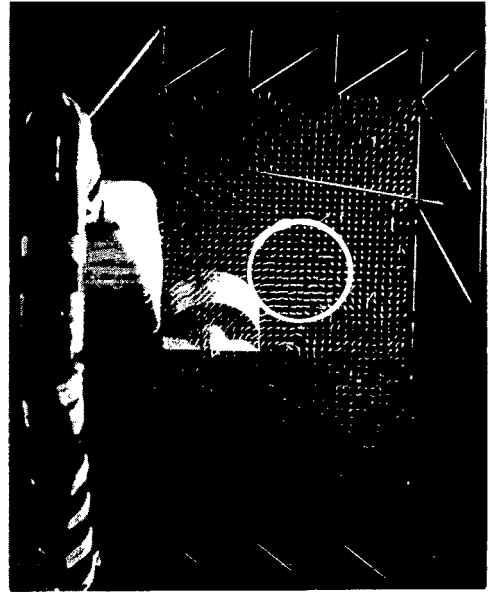
$$\alpha = 0°$$
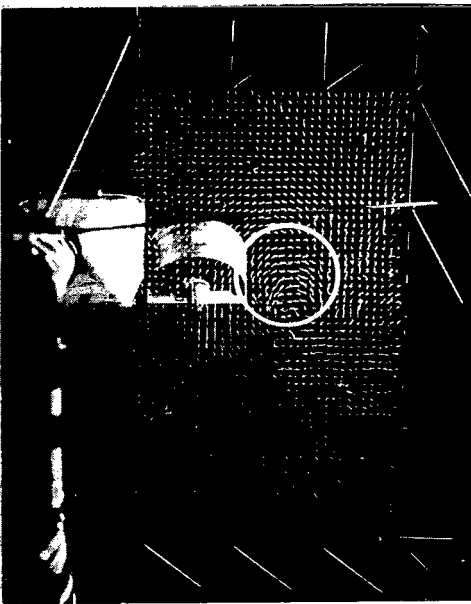
$$\alpha = 10°$$
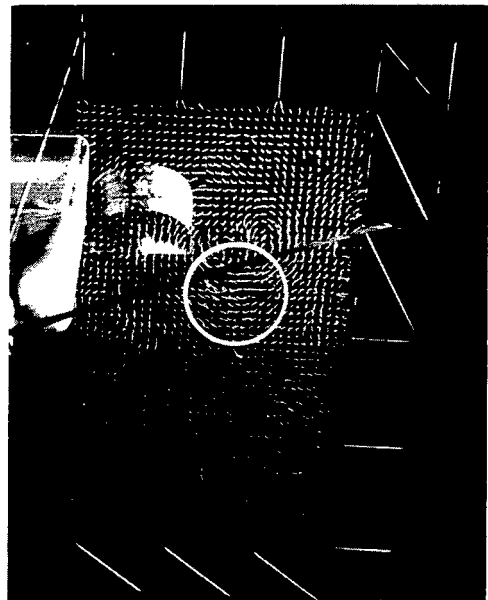
$$\alpha = 20°$$

(f) $i_d = 44°$; N = 3,679 rpm; q = 0.72; μ = 0.110.

L-63-9275

Figure 3.- Continued.
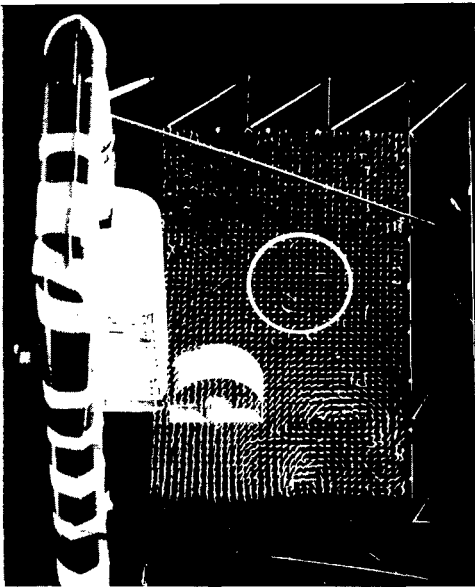
$\alpha = -10°$
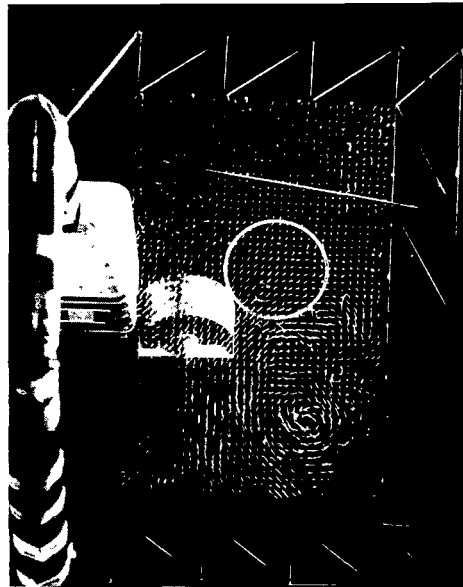
$\alpha = 0°$
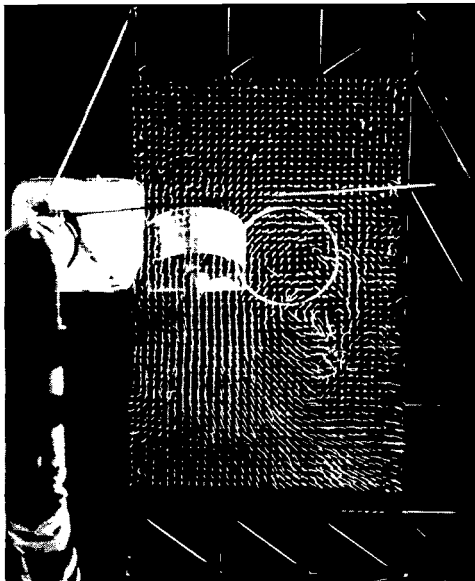
$\alpha = 10°$
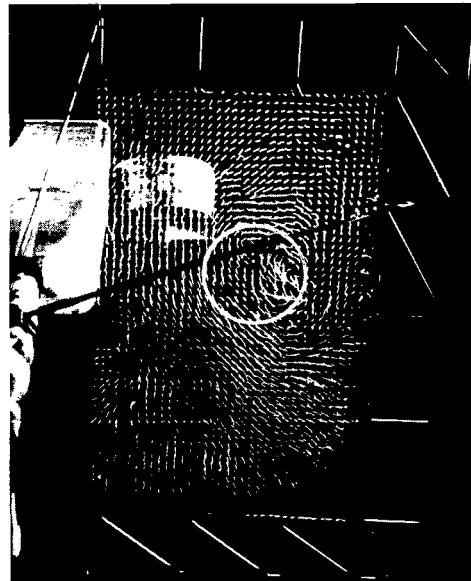
$\alpha = 20°$

(g) $i_d = 59°$; N = 3,927 rpm; q = 0.635; $\mu = 0.096$.   L-63-9276

Figure 3.- Continued.

$$a = -10°$$

$$a = O°$$

$$a = 10°$$
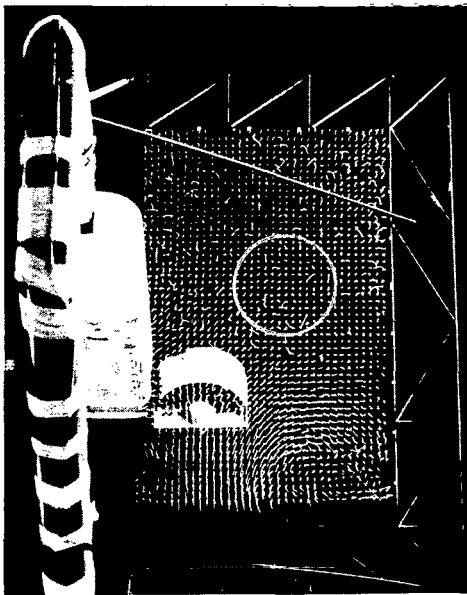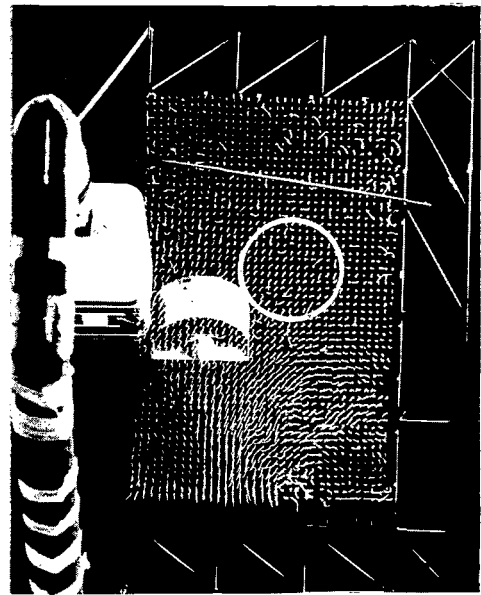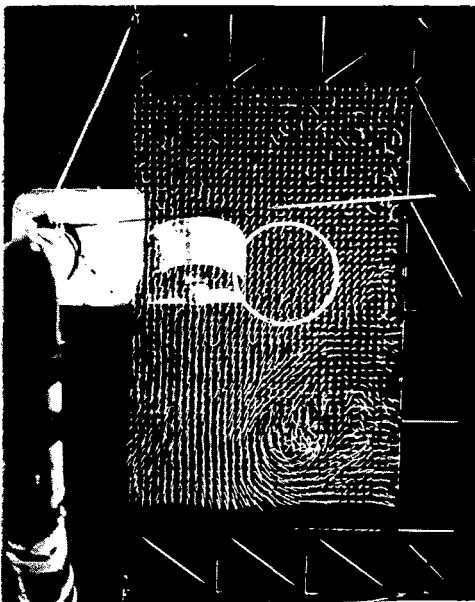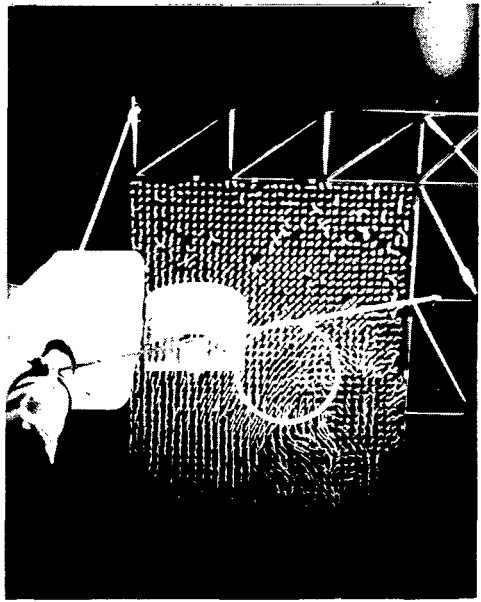
$$a = 20°$$

(h) $i_d = 59°$; N = 5,172 rpm; q = 0.635; μ = 0.073.   L-63-9277

Figure 3.- Continued.
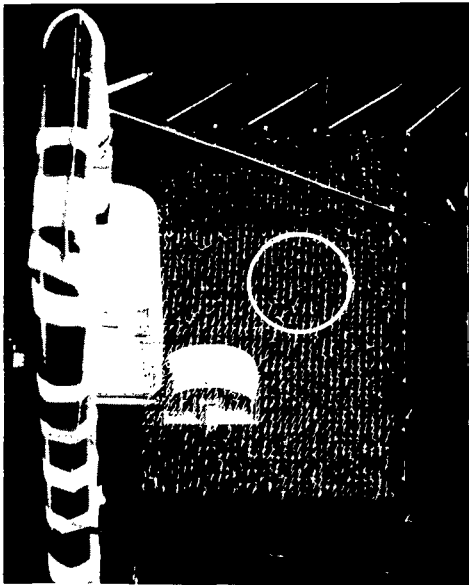
$\alpha = -10°$
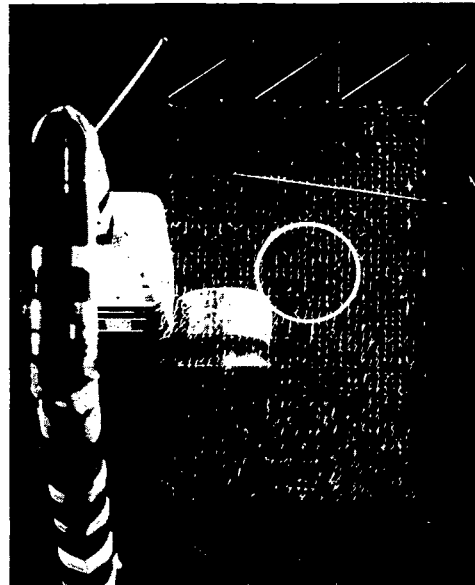
$\alpha = 0°$
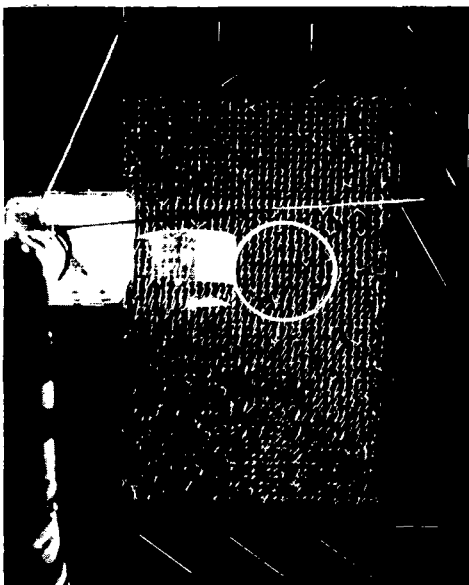
$\alpha = 10°$
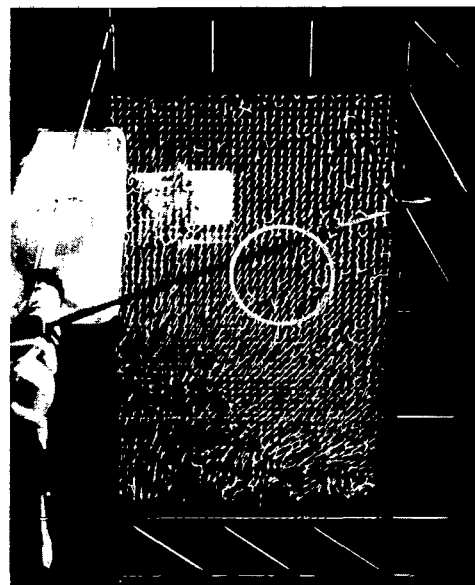
$\alpha = 20°$

(i) $i_d = 75°$; $N = 3,963$ rpm; $q = 0.2$; $\mu = 0.054$.

Figure 3.- Continued.

L-63-9278
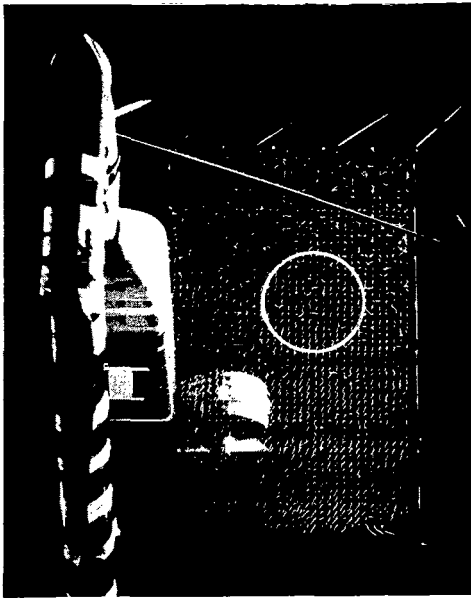
$\alpha = -10°$
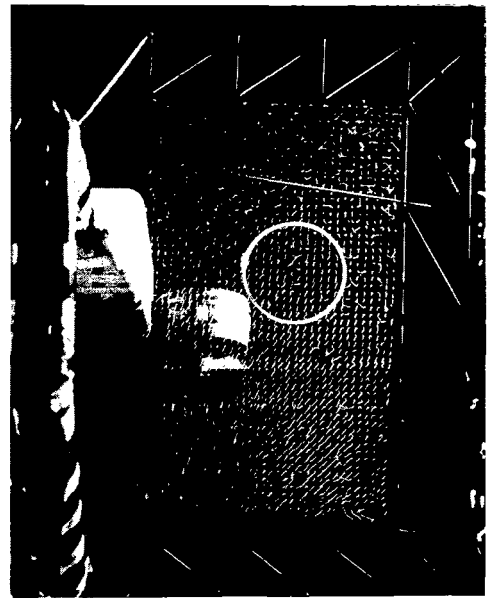
$\alpha = 0°$
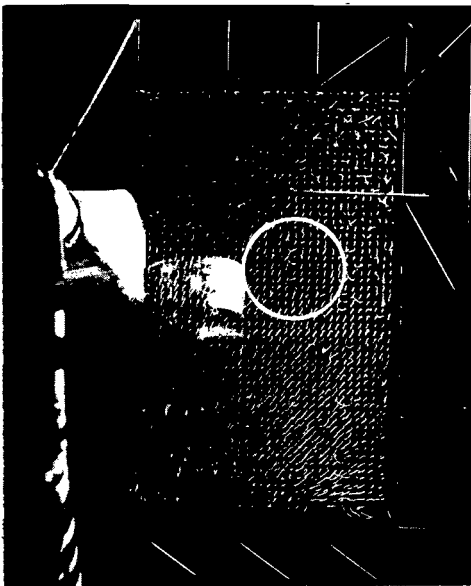
$\alpha = 10°$
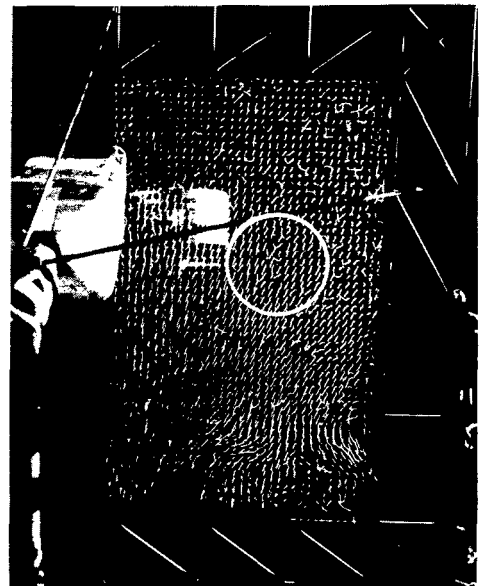
$\alpha = 20°$

(j) $i_d = 75°$; N = 5,025 rpm; q = 0.2; μ = 0.042.

L-63-9279

Figure 3.- Concluded.

	i_d, deg		q,	μ_F	μ_R	$L_{a=10°}$, lb	$\left(\dfrac{N_F}{N_R}\right)^2$
	Front	Rear	lb /ft²				
○	0	0	6.00	.26	.25	64.61	.90
□	15	16	5.99	.23	.23	90.84	.98
◇	32	32	3.17	.17	.17	78.28	.97
△	45	46	1.87	.13	.13	53.04	1.00
◁	65	60	.67	.08	.08	59.88	1.00
◁	74	77	.20	.04	.04	58.01	.99
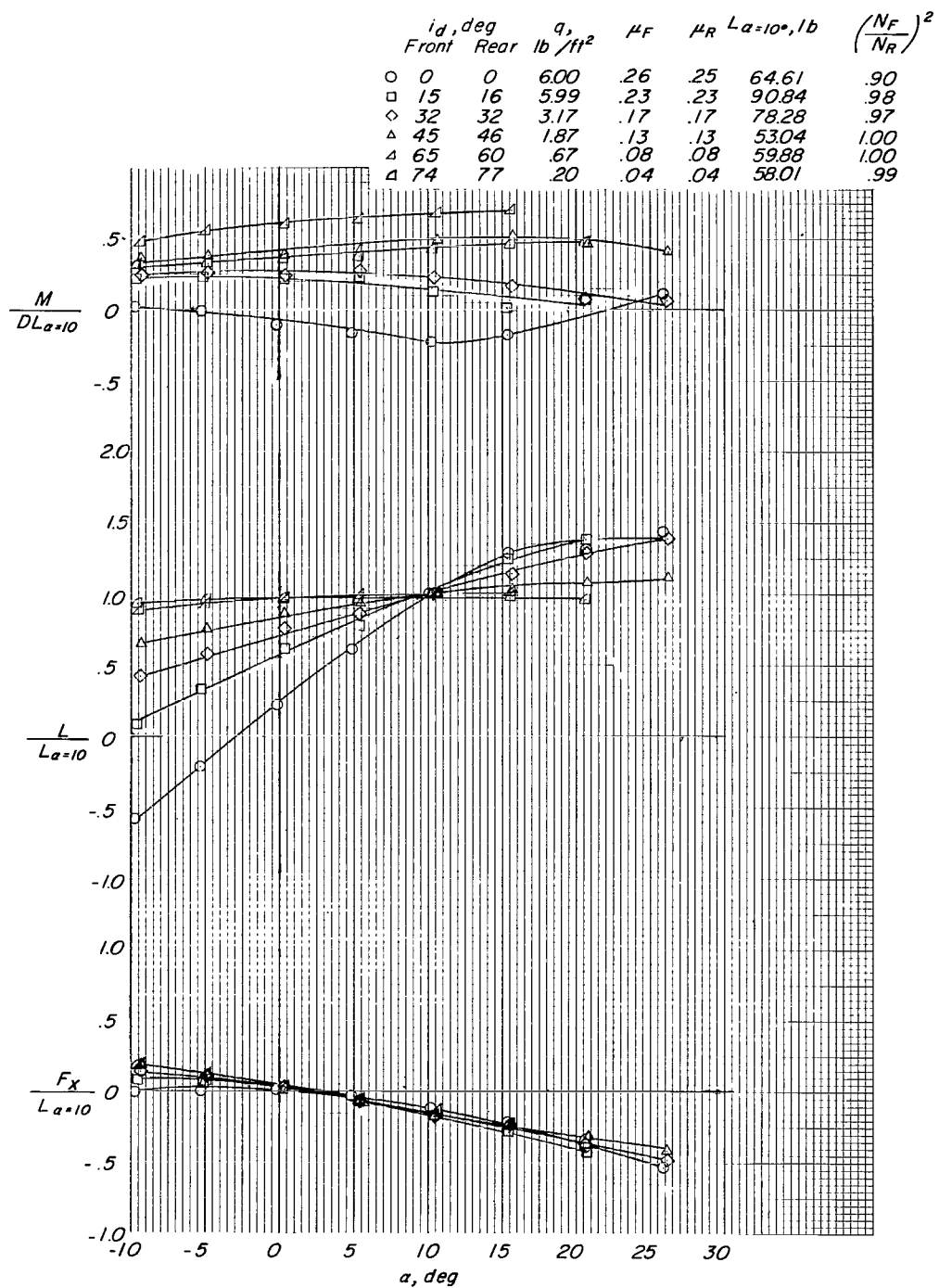
(a) Complete model.

Figure 4.- Aerodynamic characteristics of basic configuration.

21

$\frac{M}{DL_{a=10}}$

.5

0

-.5

i_d, deg		q,	μ_F	μ_R	$L_{a=10°}$, lb	$\left(\frac{N_F}{N_R}\right)^2$
Front	Rear	lb/ft²				
0	0	6.00	.26	.25	64.61	.90
15	16	5.99	.23	.23	90.84	.98
32	32	3.17	.17	.17	78.28	.97
45	46	1.87	.13	.13	53.04	1.00
65	60	.67	.08	.08	59.88	1.00
74	77	.20	.04	.04	58.01	.99

1.0

$\frac{L}{L_{a=10}}$

.5

0

-.5

-1.0

.5

$\frac{F_X}{L_{a=10}}$

0

-.5

-1.0

-10 -5 0 5 10 15 20 25 30

a, deg
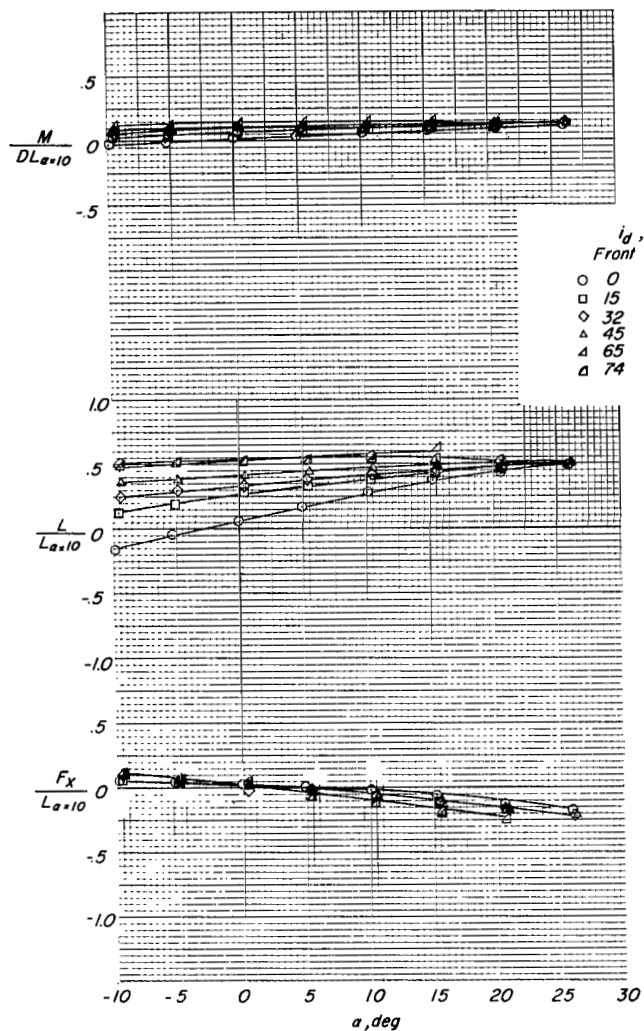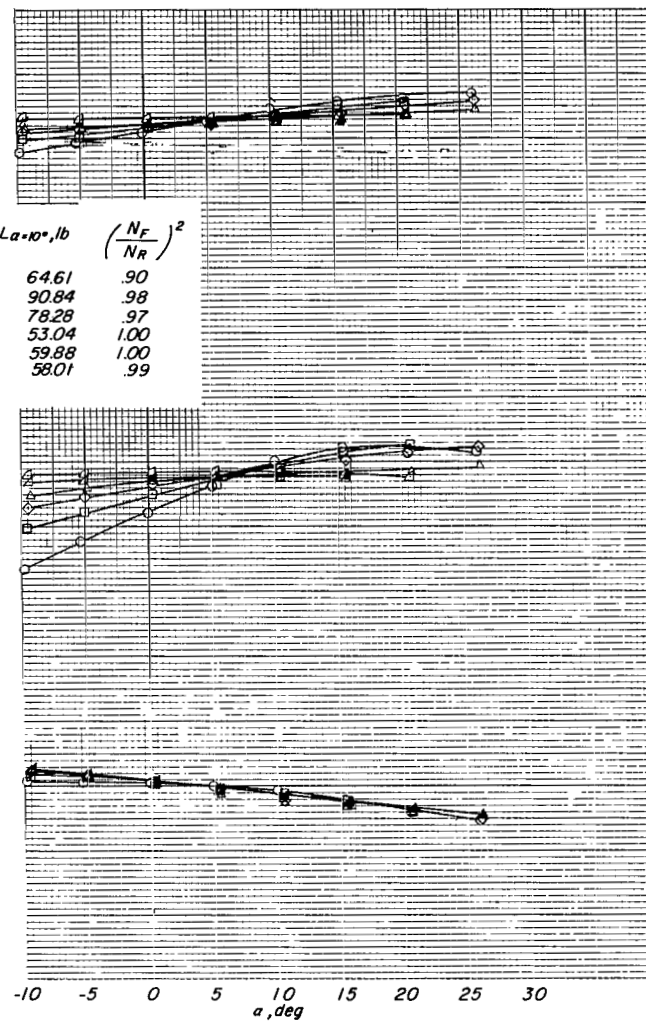
(b) Front ducts.

(c) Rear ducts.

Figure 4.- Concluded.

	i_d, deg		q,	μ_F	μ_R	$L_{a=10°}$, lb	$\left(\dfrac{N_F}{N_R}\right)^2$
	Front	Rear	lb /ft²				
○	2	32	4.34	.20	.20	78.72	.99
□	15	32	4.05	.19	.19	84.49	1.00
◇	32	32	3.17	.17	.17	78.28	.97

$\dfrac{M}{D L_{a=10}}$

$\dfrac{L}{L_{a=10}}$

$\dfrac{F_x}{L_{a=10}}$

a, deg
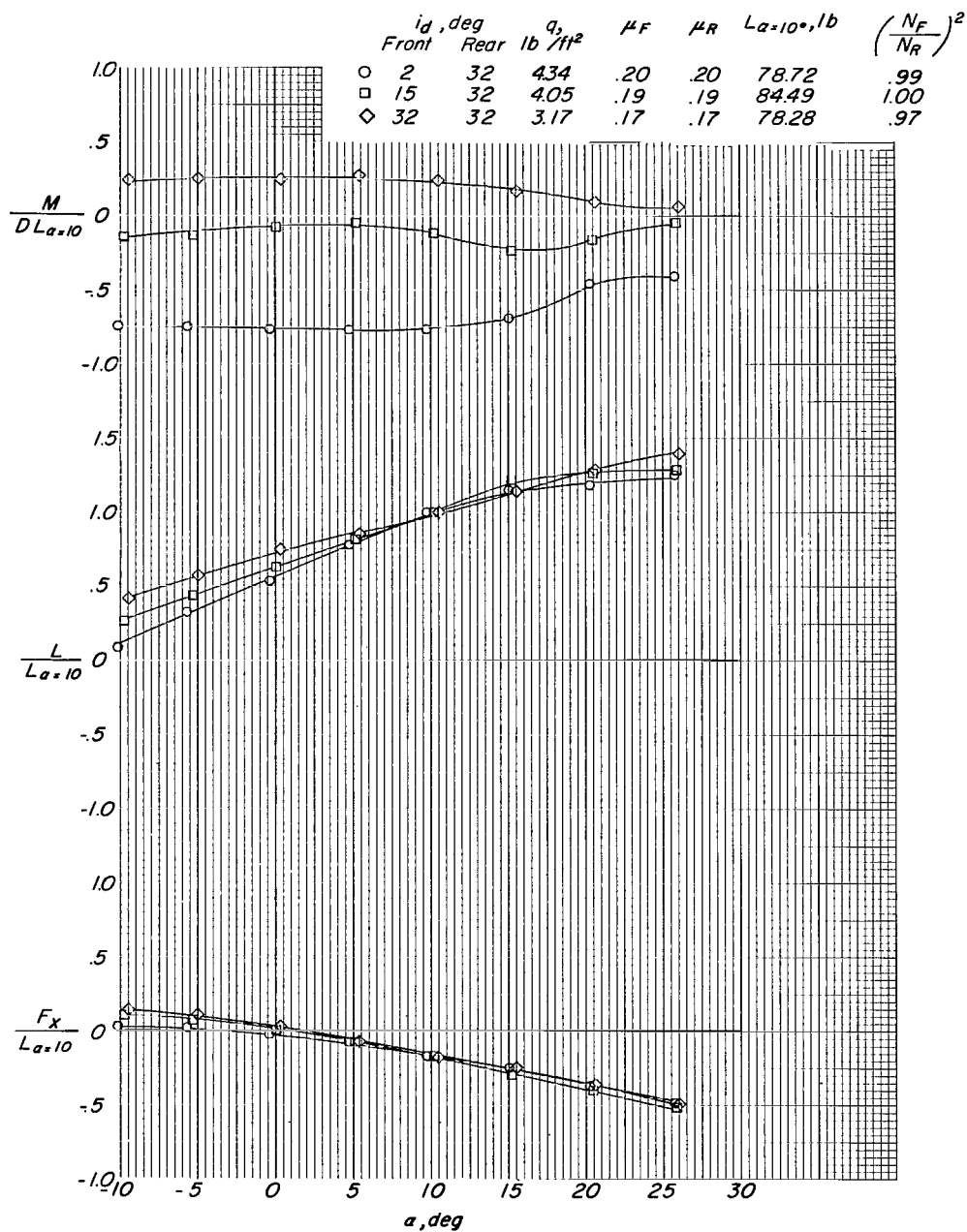
(a) Complete model.

Figure 5.- Aerodynamic characteristics with differential duct incidence. $i_{d,R} = 32°$.

23

	i_d ,deg		q_1	μ_F	μ_R	$L_{a=10°}$,lb	$\left(\dfrac{N_F}{N_R}\right)^2$
	Front	Rear	lb /ft²				
○	2	32	4.34	.20	.20	78.72	.99
□	15	32	4.05	.19	.19	84.49	1.00
◇	32	32	3.17	.17	.17	78.28	.97
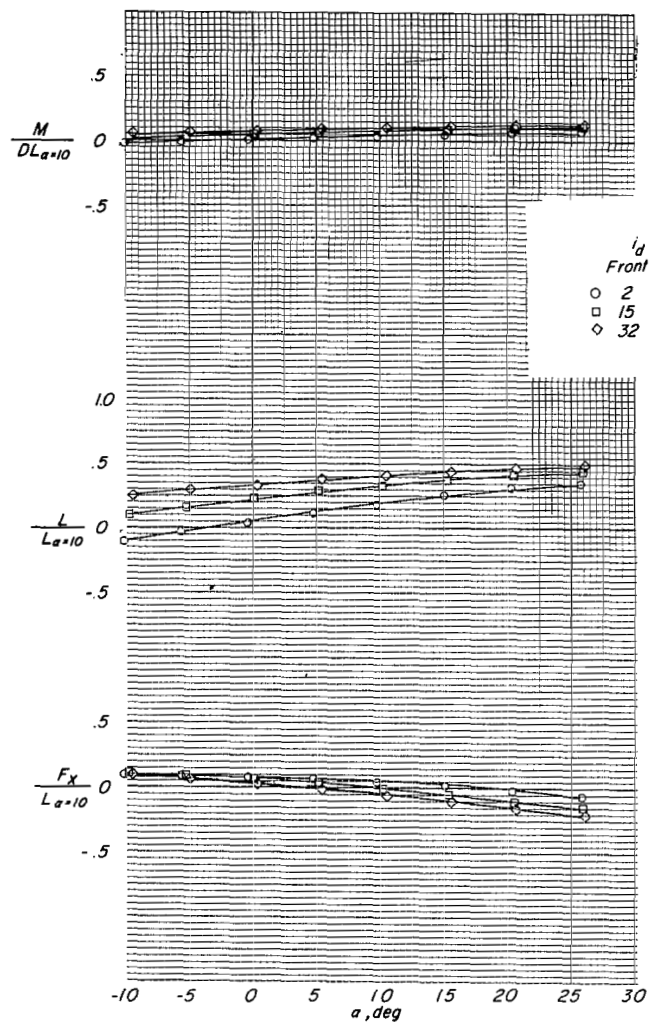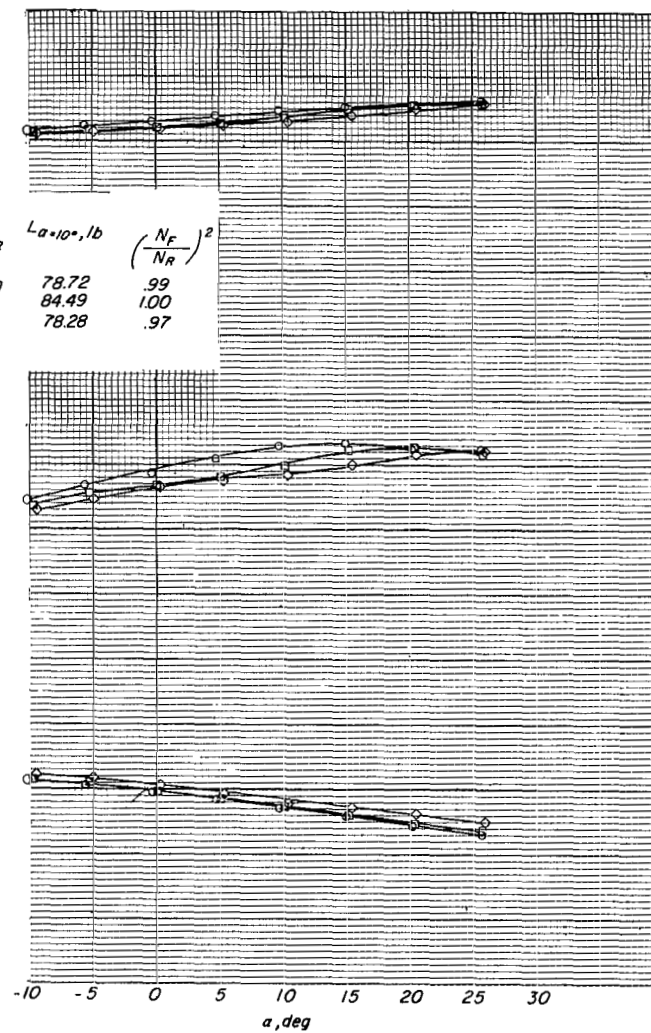
(b) Front ducts.

(c) Rear ducts.

Figure 5.- Concluded.

	i_d, deg		q,	μ_F	μ_R	$L_{a=10°}$, lb	$\left(\dfrac{N_F}{N_R}\right)^2$
	Front	Rear	lb /ft²				
○	15	46	2.82	.16	.16	76.49	1.00
□	31	46	2.40	.15	.15	75.76	1.00
◇	45	46	1.87	.13	.13	53.04	1.00
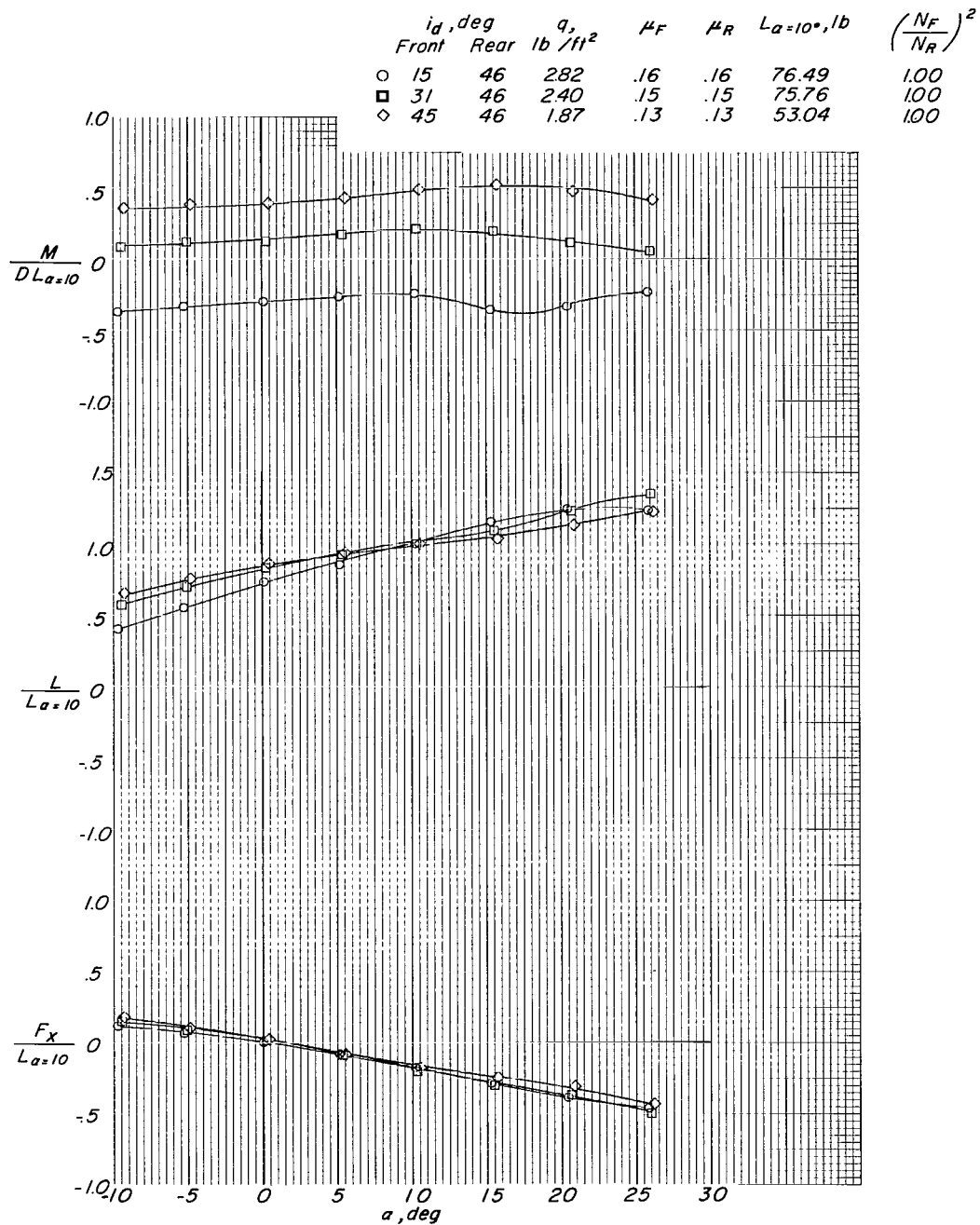
(a) Complete model.

Figure 6.- Aerodynamic characteristics with differential duct incidence. $i_{d,R} = 46°$.

	i_d, deg		q,	μ_F	μ_R	$L_{a=10°}$, lb	$\left(\dfrac{N_F}{N_R}\right)^2$
	Front	Rear	lb/ft²				
○	15	46	2.82	.16	.16	76.49	1.00
□	31	46	2.40	.15	.15	75.76	1.00
◇	45	46	1.87	.13	.13	53.04	1.00
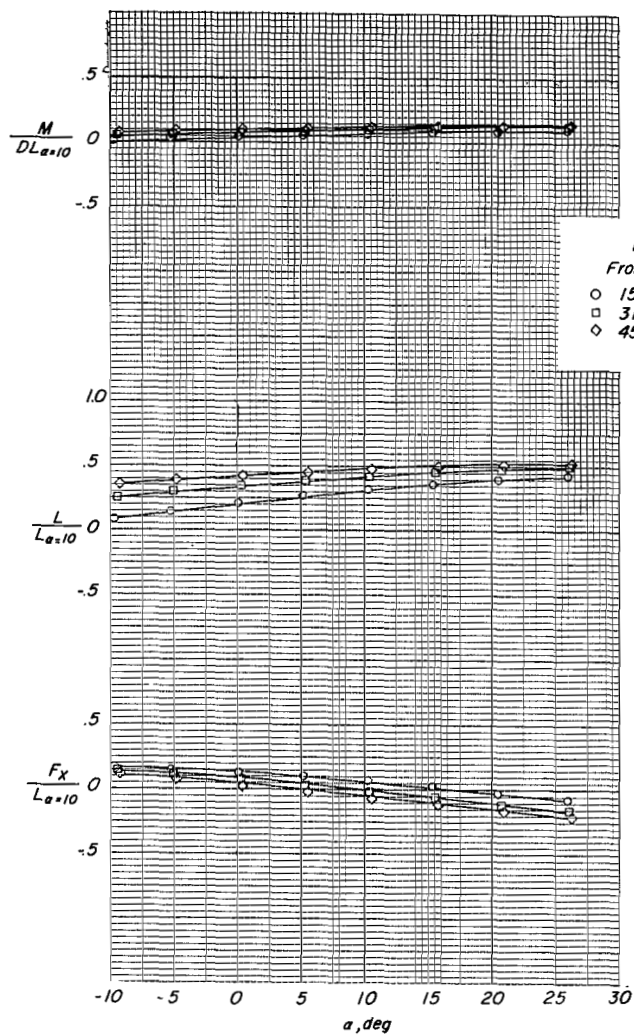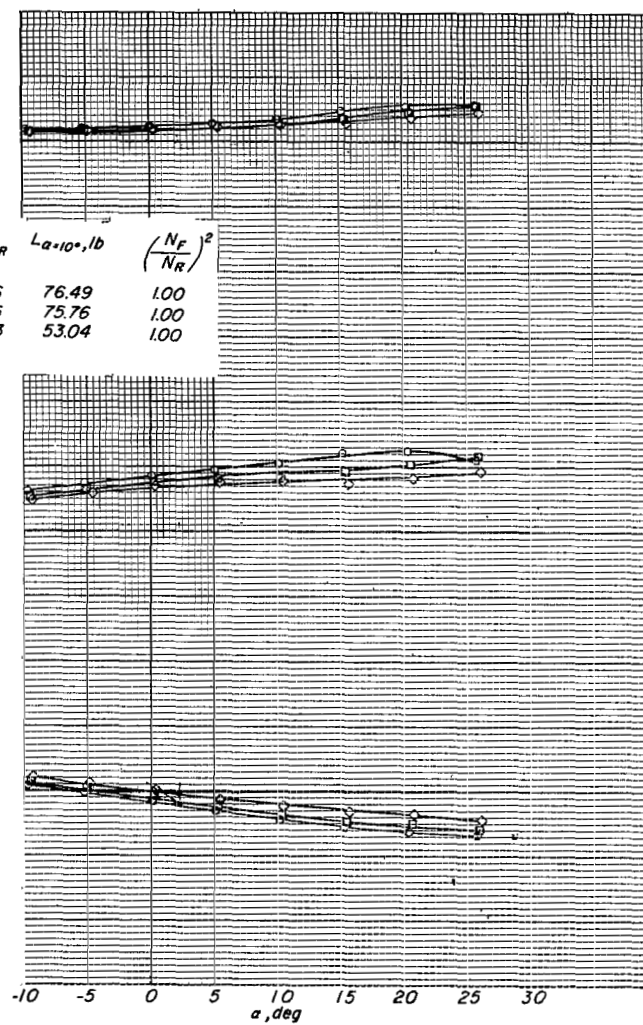
(b) Front ducts.

(c) Rear ducts.

Figure 6.- Concluded.

	i_d, deg		q,	μ_F	μ_R	$L_{a=10°}$, lb	$\left(\dfrac{N_F}{N_R}\right)^2$
	Front	Rear	lb/ft²				
○	30	60	1.57	.12	.12	65.26	.99
□	45	60	1.22	.11	.11	64.74	1.00
◇	63	60	.67	.08	.08	59.88	1.00
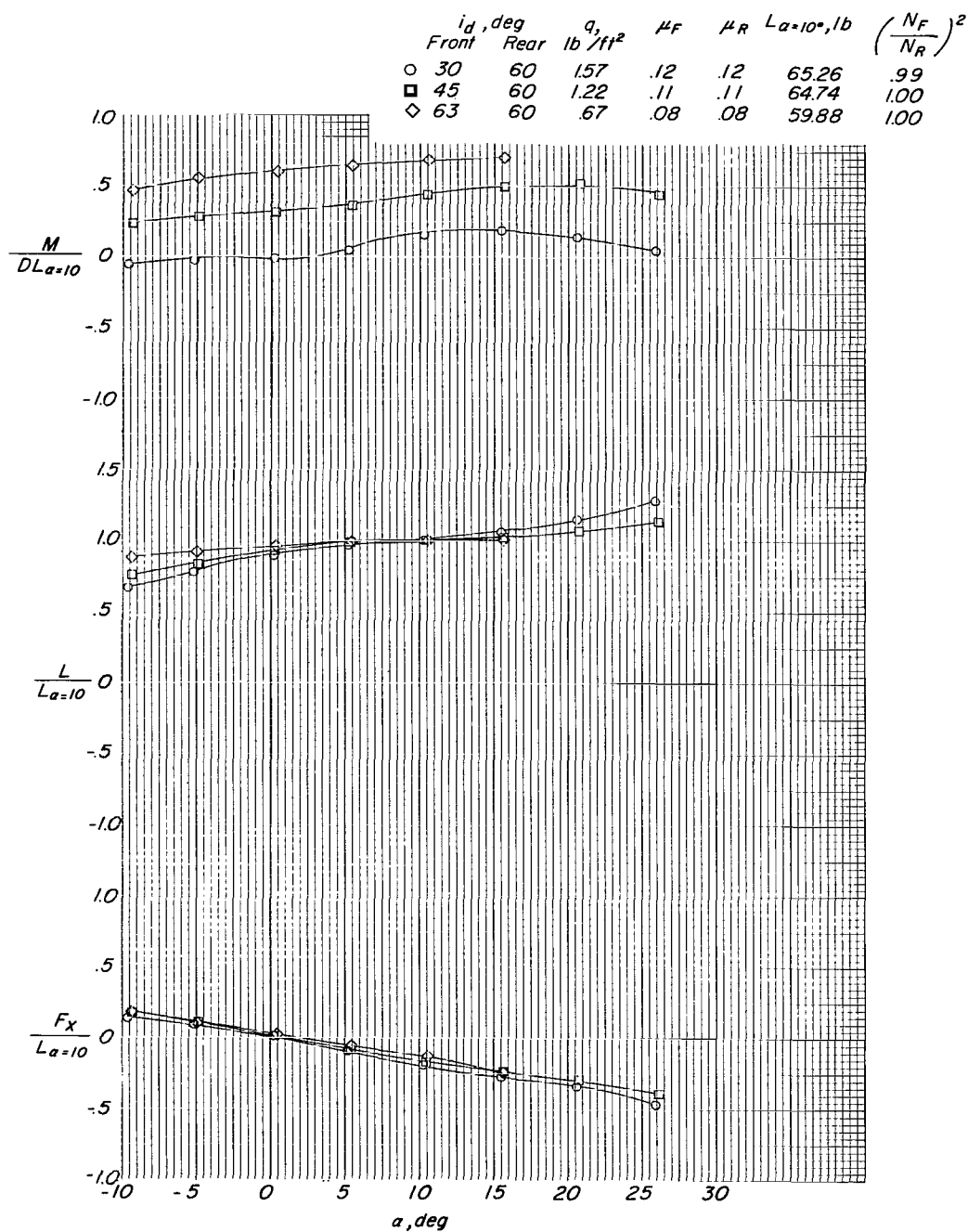
(a) Complete model.

Figure 7.- Aerodynamic characteristics with differential duct incidence. $i_{d,R} = 60°$.
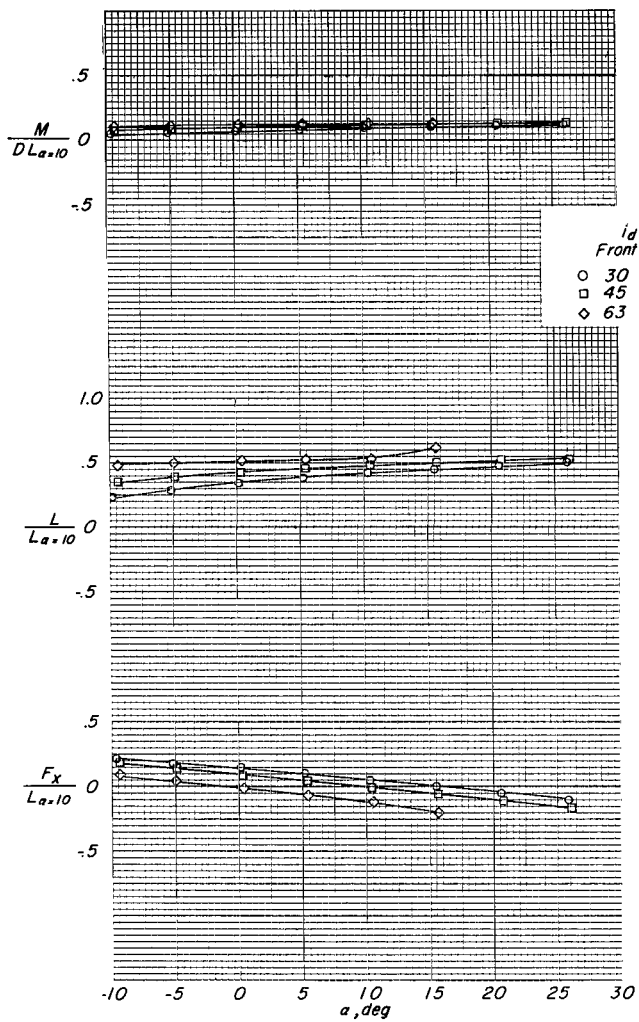
(b) Front ducts.
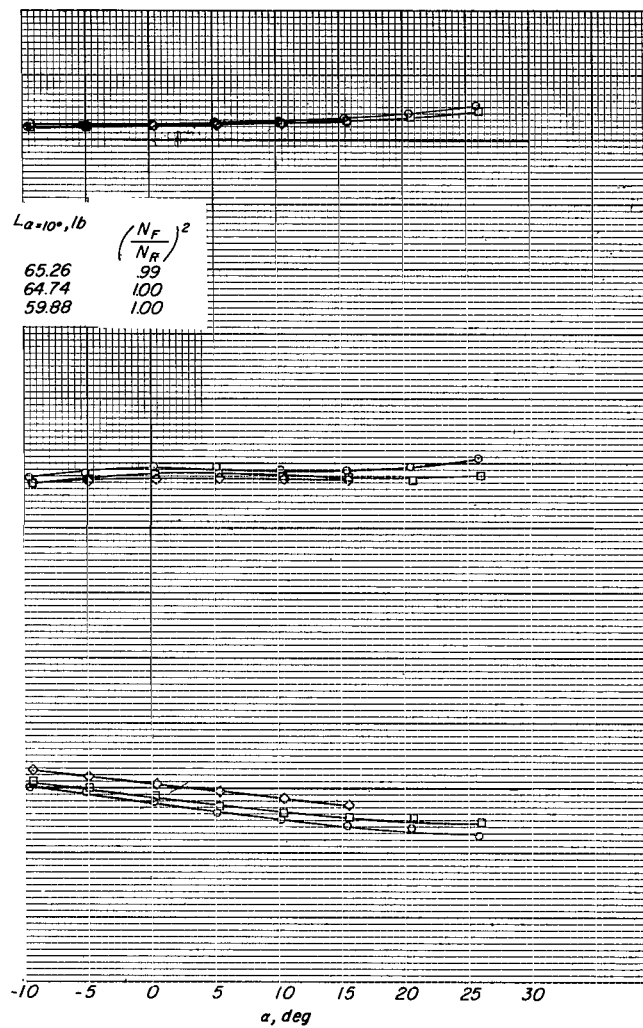
(c) Rear ducts.

Figure 7.- Concluded.

| | i_d, deg | | q, | | | $L_{a=10}$, lb | $\left(\dfrac{N_F}{N_R}\right)^2$ |
	Front	Rear	lb /ft^2	μ_F	μ_R		
○	15	77	.20	.10	.10	49.17	.99
⊐	32	77	1.02	.10	.10	58.51	.99
◇	43	77	.69	.08	.08	58.27	.99
△	63	77	.50	.07	.07	55.33	.96
◿	74	77	.20	.04	.04	58.01	.99
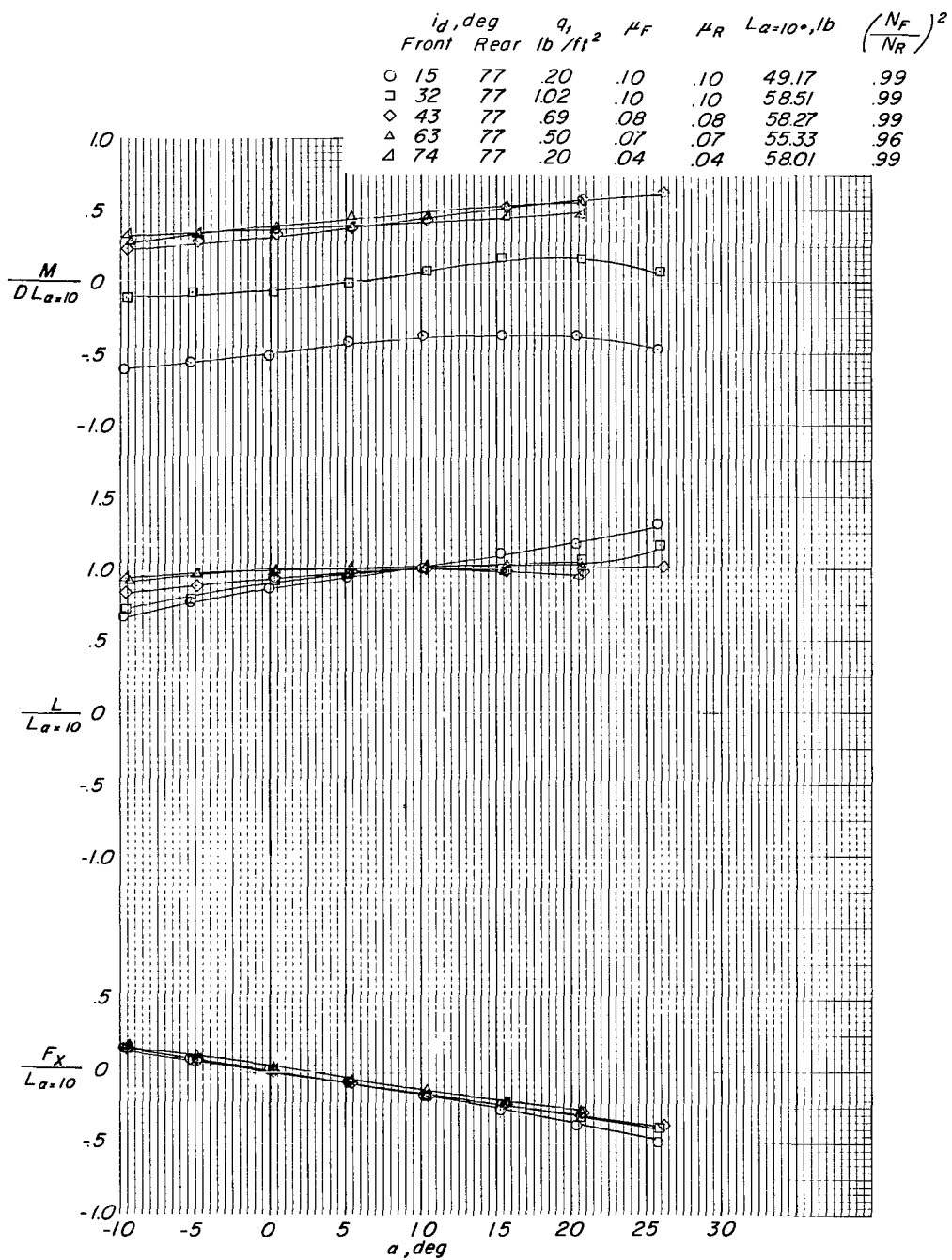
(a) Complete model.

Figure 8.- Aerodynamic characteristics with differential duct incidence. $i_{d,R}$ = 77°.

	i_d, deg		q,	μ_F	μ_R	$L_{a=10°}$, lb	$\left(\dfrac{N_F}{N_R}\right)^2$
	Front	Rear	lb/ft²				
○	15	77	.20	.10	.10	49.17	.99
□	32	77	1.02	.10	.10	58.51	.99
◇	43	77	.69	.08	.08	58.27	.99
△	63	77	.50	.07	.07	55.33	.96
◁	74	77	.20	.04	.04	58.01	.99
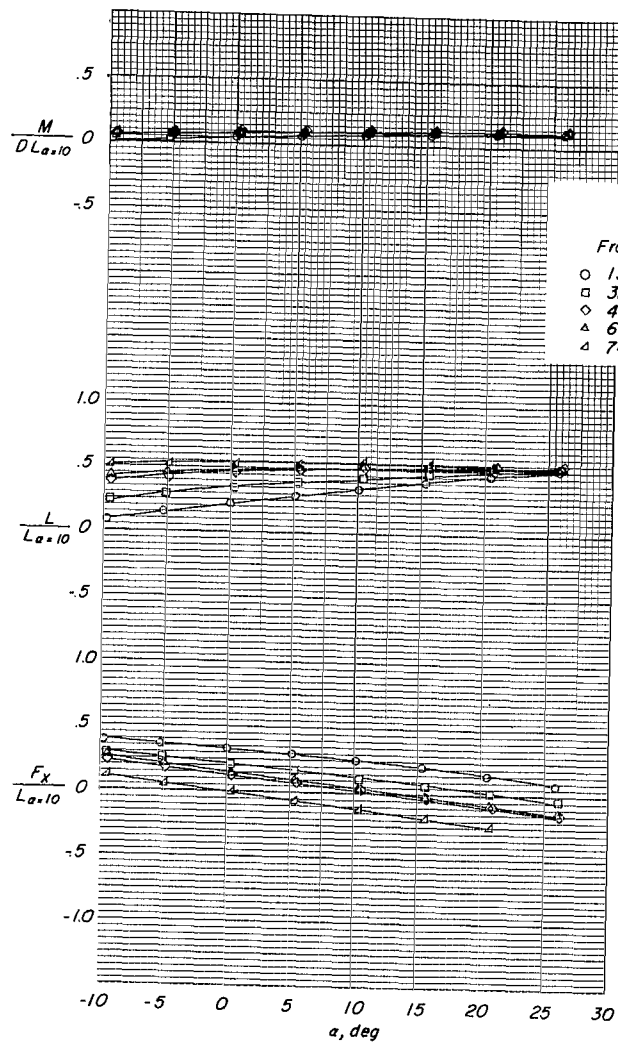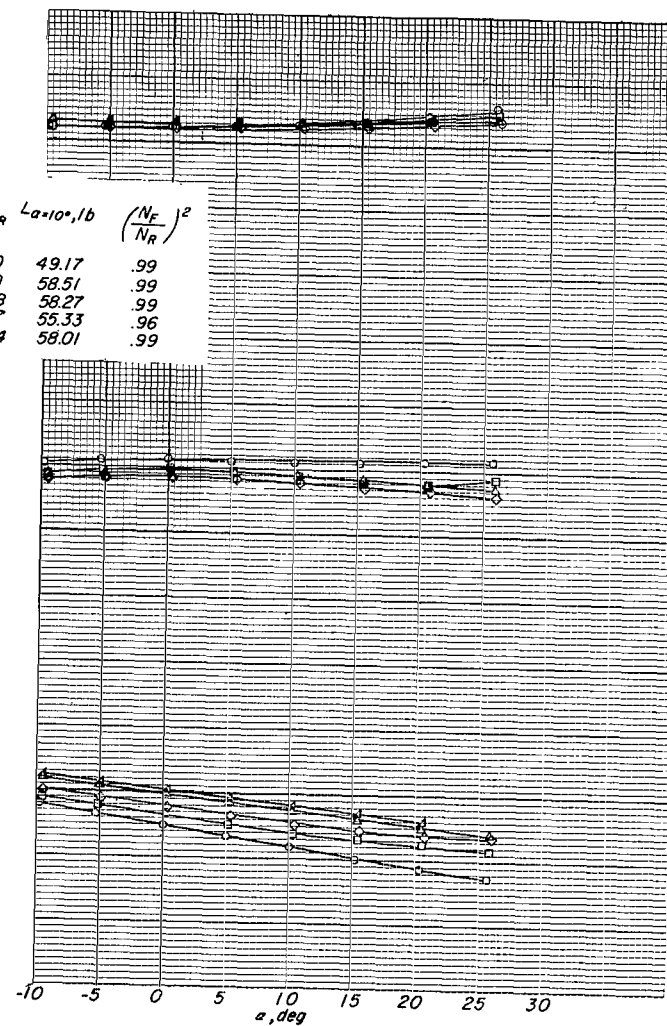
(b) Front ducts.

(c) Rear ducts.

Figure 8.- Concluded.

	i_d, deg		q,	μ_F	μ_R	$L_{a=10°}$, lb	$\left(\dfrac{N_F}{N_R}\right)^2$
	Front	Rear	lb/ft²				
○	29	31	3.52	.20	.17	88.76	.71
□	29	31	3.52	.20	.17	86.83	.79
◇	29	31	3.52	.19	.18	85.80	.86
△	32	32	3.17	.17	.17	78.28	.97
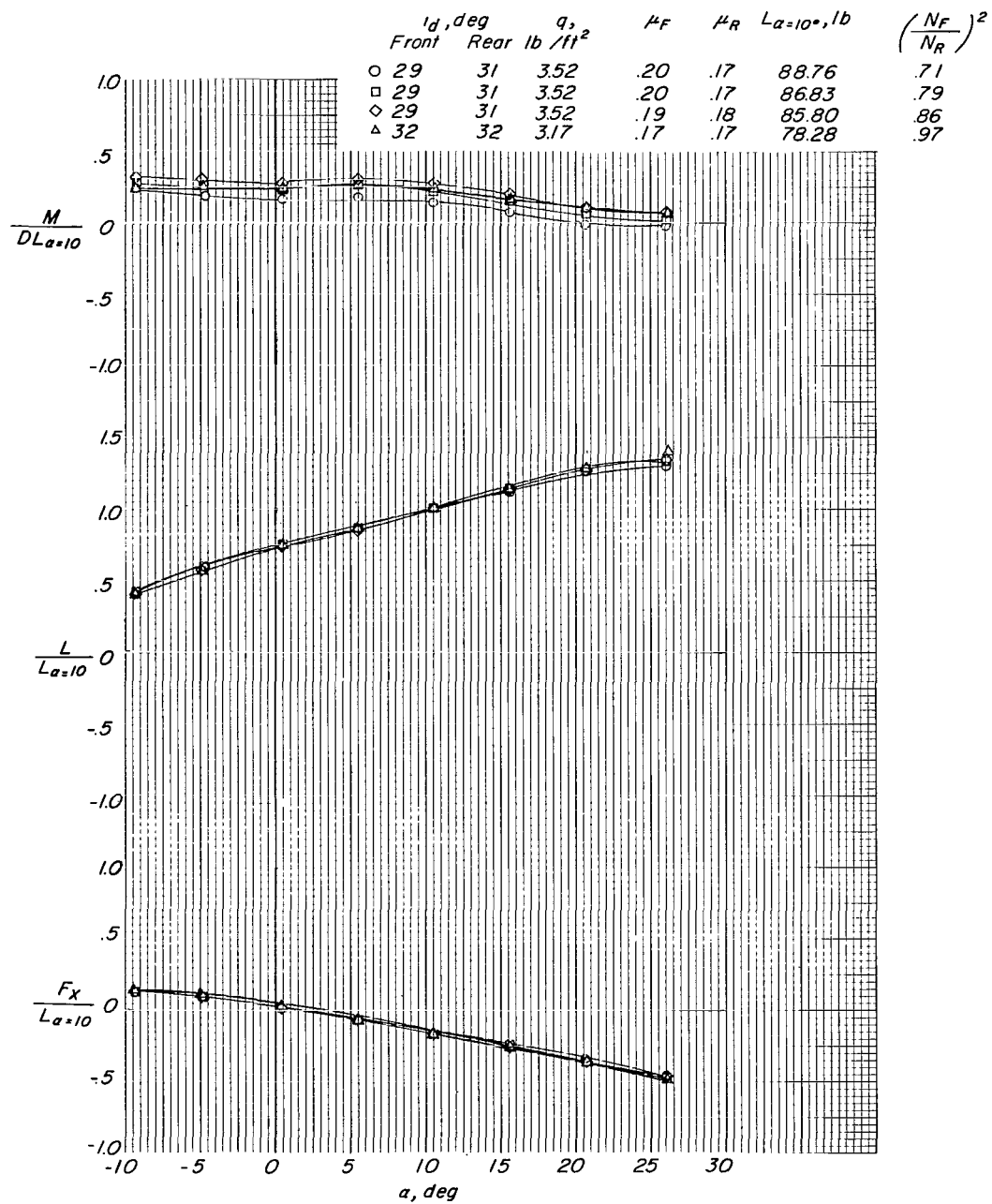
(a) Complete model.

Figure 9.- Aerodynamic characteristics with differential thrust. $i_d \approx 30°$.

	i_d, deg		q,	μ_F	μ_R	$La_{=10}$, lb	$\left(\dfrac{N_F}{N_R}\right)^2$
	Front	Rear	lb /ft²				
○	29	31	3.52	.20	.17	88.76	.71
□	29	31	3.52	.20	.17	86.83	.79
◇	29	31	3.52	.19	.18	85.80	.86
△	32	32	3.17	.17	.17	78.28	.97
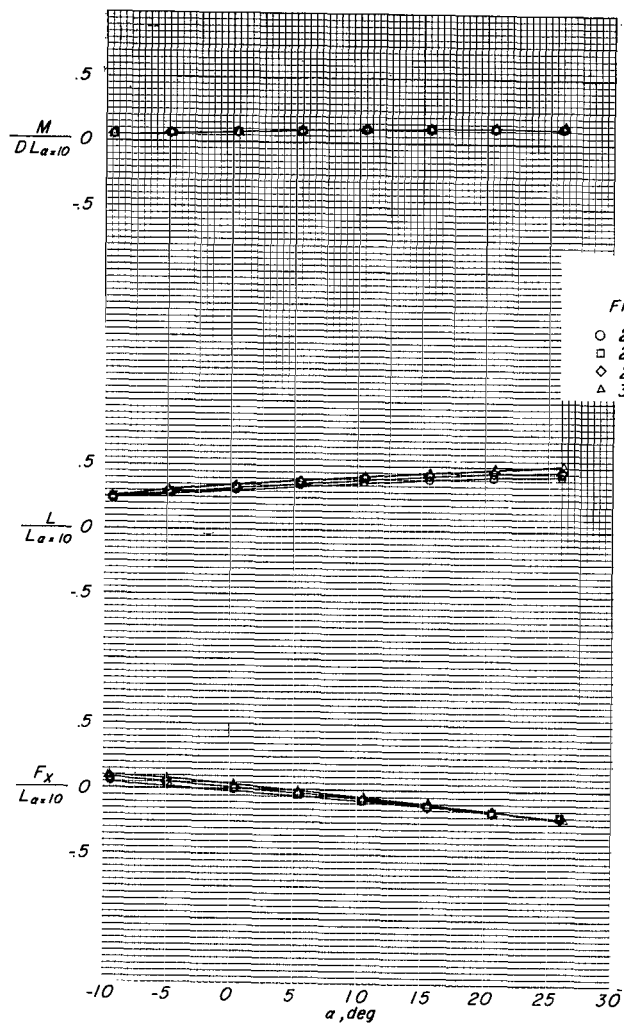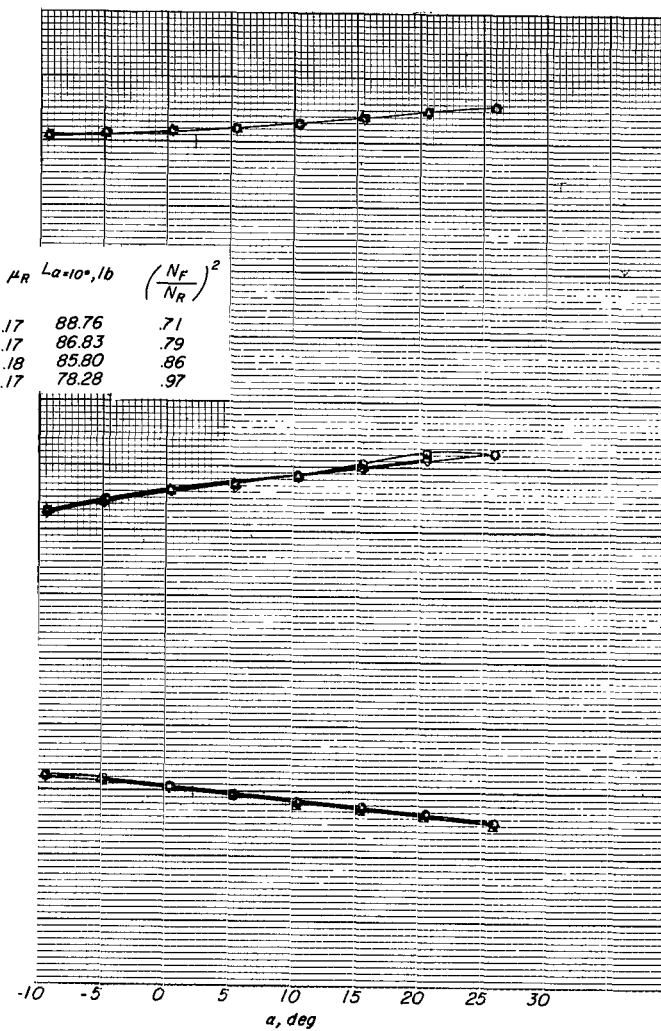
(b) Front ducts.　　　　　　　　　　　　　　(c) Rear ducts.

Figure 9.- Concluded.

	i_d, deg		q,	μ_F	μ_R	$L_{a=10°}$, lb	$\left(\dfrac{N_F}{N_R}\right)^2$
	Front	Rear	lb/ft²				
○	46	44	1.48	.16	.13	54.88	.61
□	46	44	1.48	.15	.13	55.52	.76
◇	46	44	1.48	.15	.13	54.23	.74
△	46	44	1.48	.15	.13	55.55	.72
◁	45	46	1.87	.13	.13	73.04	1.00
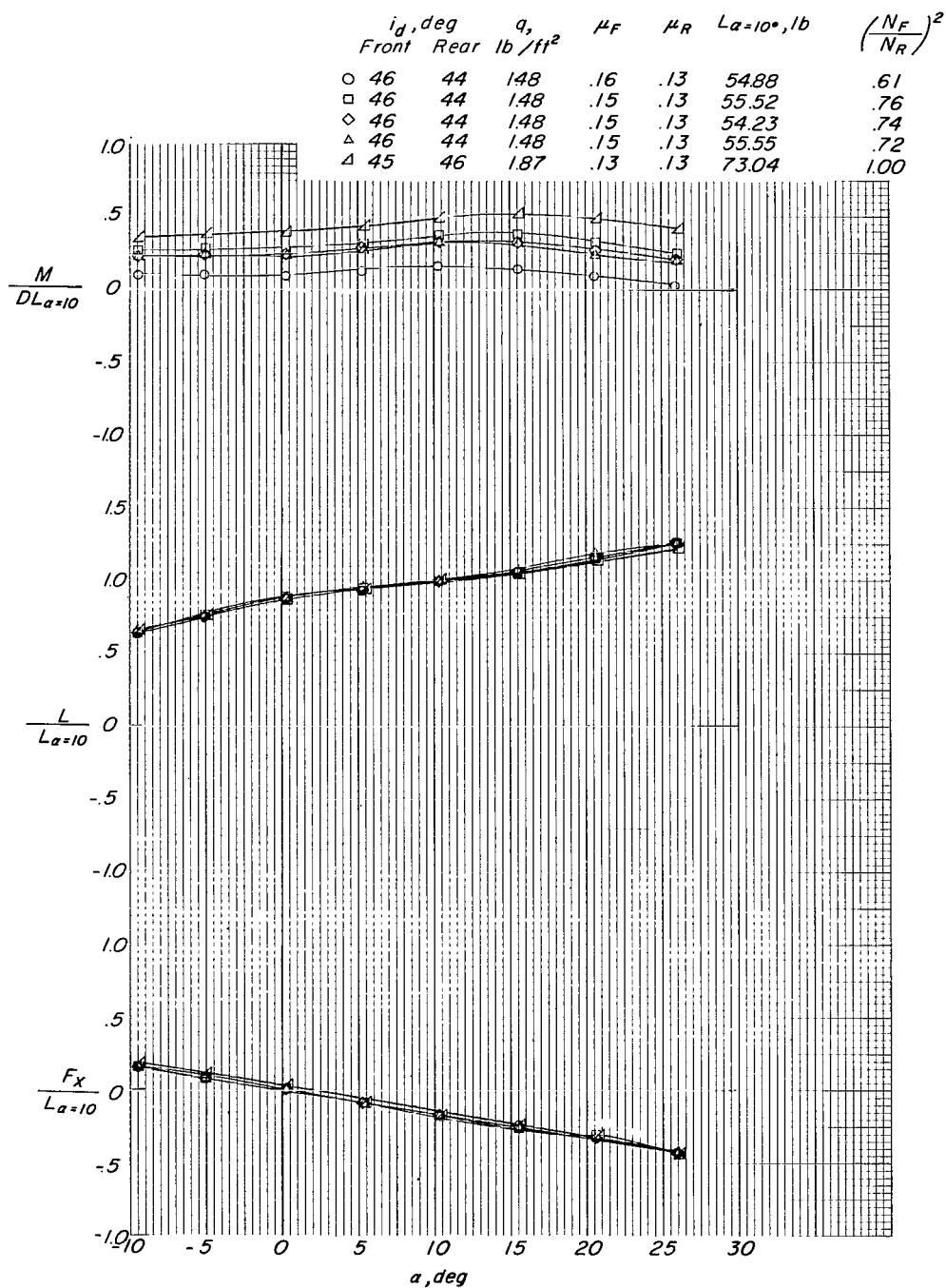
(a) Complete model.

Figure 10.- Aerodynamic characteristics with differential thrust. $i_d \approx 45°$.

	i_d, deg		q,	μ_F	μ_R	$L_{a=10}$, lb	$\left(\dfrac{N_F}{N_R}\right)^2$
	Front	Rear	lb/ft²				
○	46	44	1.48	.16	.13	54.88	.61
□	46	44	1.48	.15	.13	55.52	.76
◇	46	44	1.48	.15	.13	54.23	.74
△	46	44	1.48	.15	.13	55.55	.72
△	45	46	1.87	.13	.13	73.04	1.00
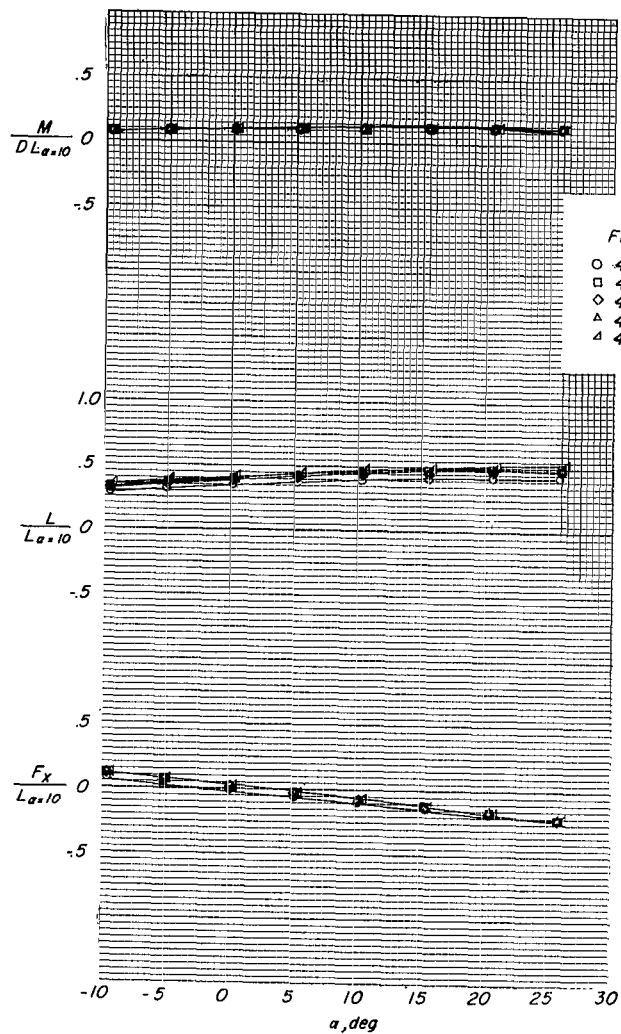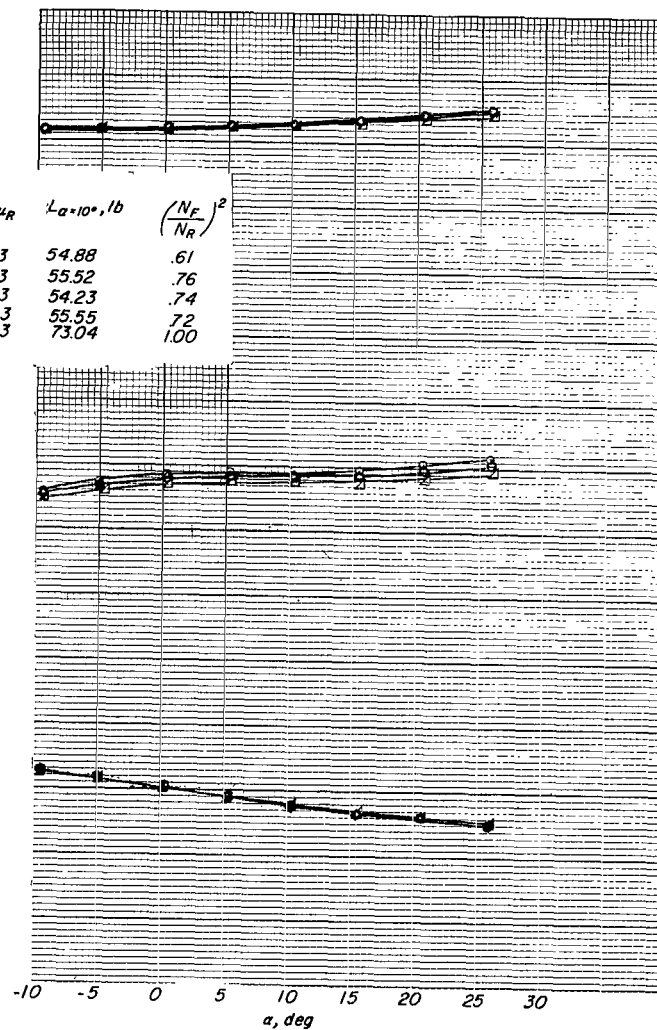
(b) Front ducts.

(c) Rear ducts.

Figure 10.- Concluded.

$$\frac{M}{DL_{a=10}}$$

	i_d, deg Front	Rear	q, lb/ft²	μ_F	μ_R	$L_{a=10°}$, lb	$\left(\dfrac{N_F}{N_R}\right)^2$
○	58	60	.50	.09	.07	46.55	.62
□	58	60	.50	.09	.07	43.15	.73
◇	58	60	.50	.09	.08	43.73	.86
△	63	60	.67	.08	.08	59.88	1.00

$$\frac{L}{L_{a=10}}$$

$$\frac{F_x}{L_{a=10}}$$

a, deg
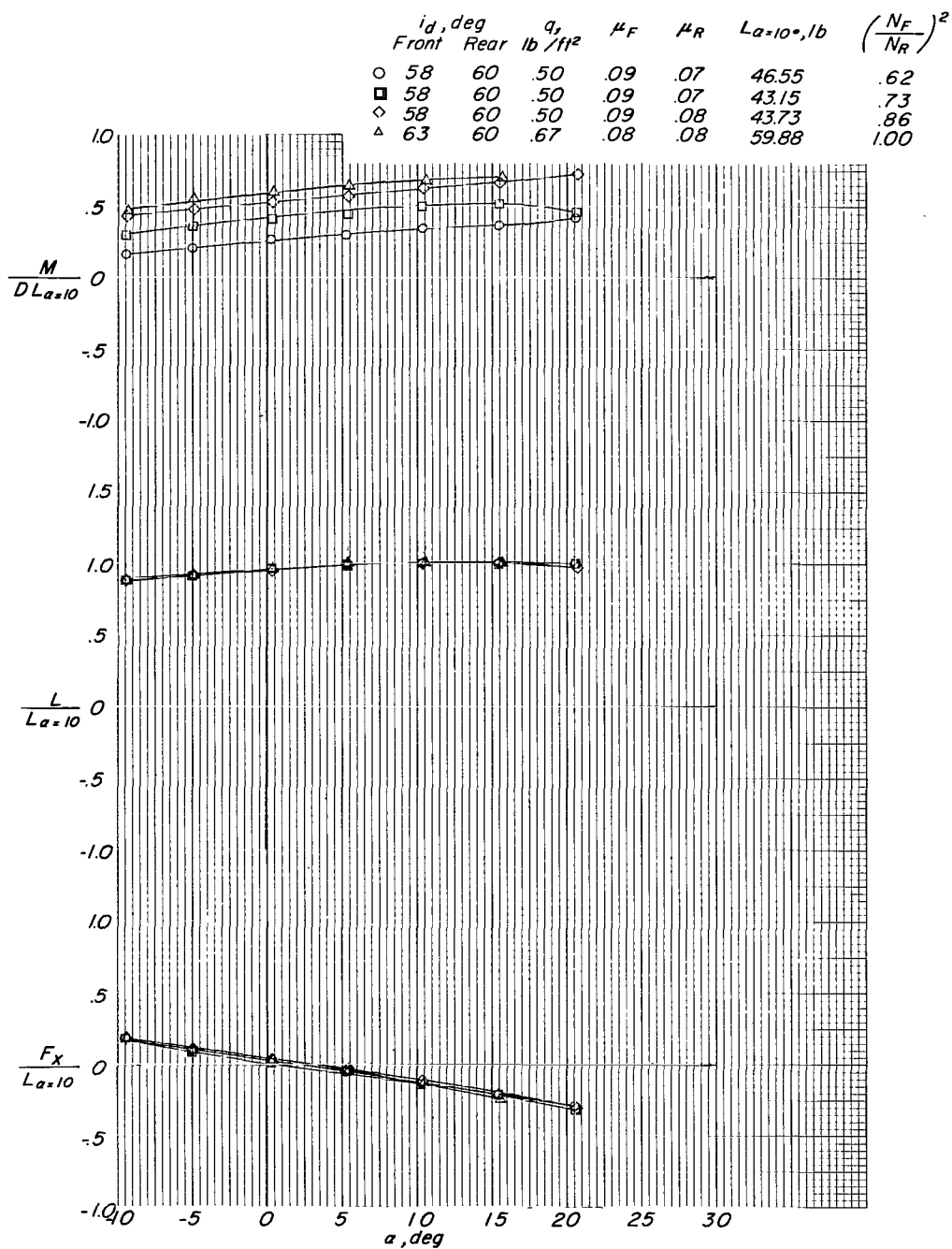
(a) Complete model.

Figure 11.- Aerodynamic characteristics with differential thrust. $i_d \approx 60°$.

	i_d,deg		q,	μ_F	μ_R	$L_{a=10°}$,lb	$\left(\dfrac{N_F}{N_R}\right)^2$
	Front	Rear	lb/ft²				
○	58	60	.50	.09	.07	46.55	.62
□	58	60	.50	.09	.07	43.15	.73
◇	58	60	.50	.09	.08	43.73	.86
△	63	60	.67	.08	.08	59.88	1.00
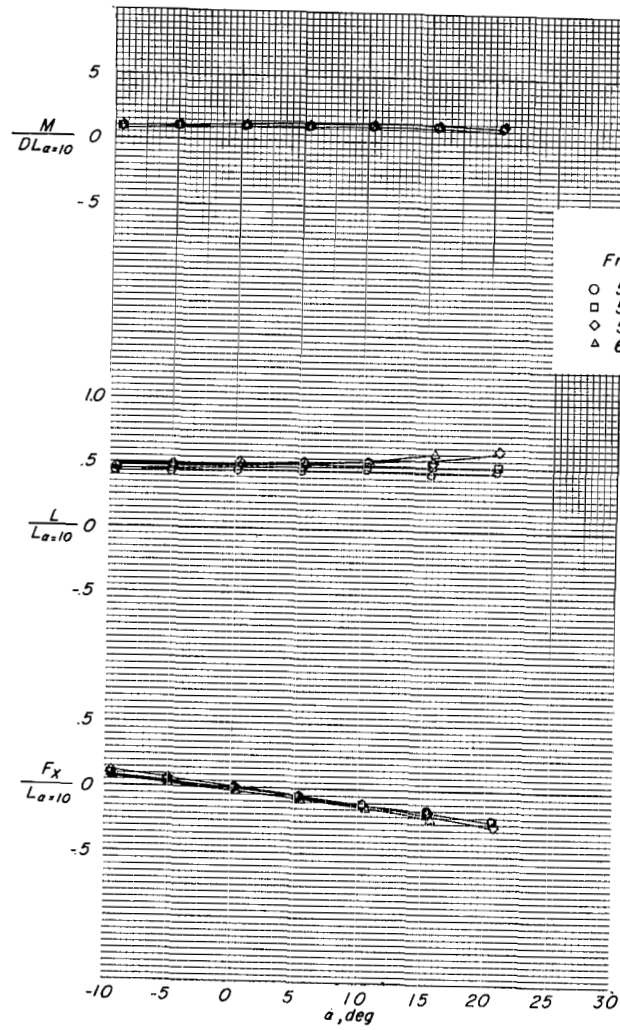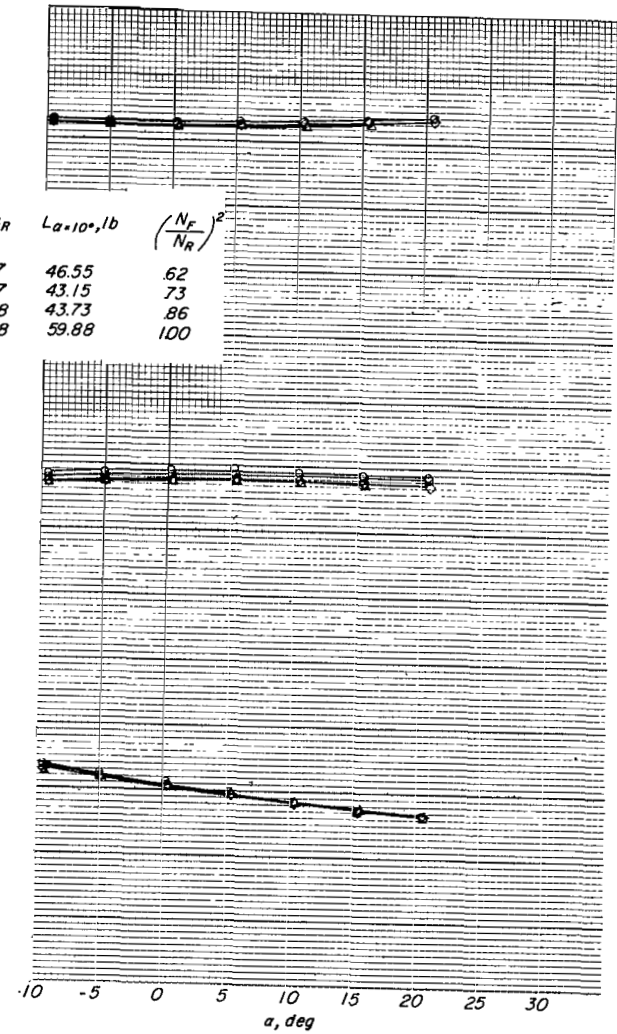
(b) Front ducts.

(c) Rear ducts.

Figure 11.- Concluded.

	i_d , deg		q,	μ_F	μ_R	$L_{a=10°}$, lb	$\left(\dfrac{N_F}{N_R}\right)^2$
	Front	Rear	lb/ft^2				
○	74	74	.25	.06	.04	59.30	.54
□	74	74	.20	.06	.04	44.29	.60
◇	74	74	.20	.05	.05	43.20	.79
△	74	77	.20	.04	.04	58.01	.99
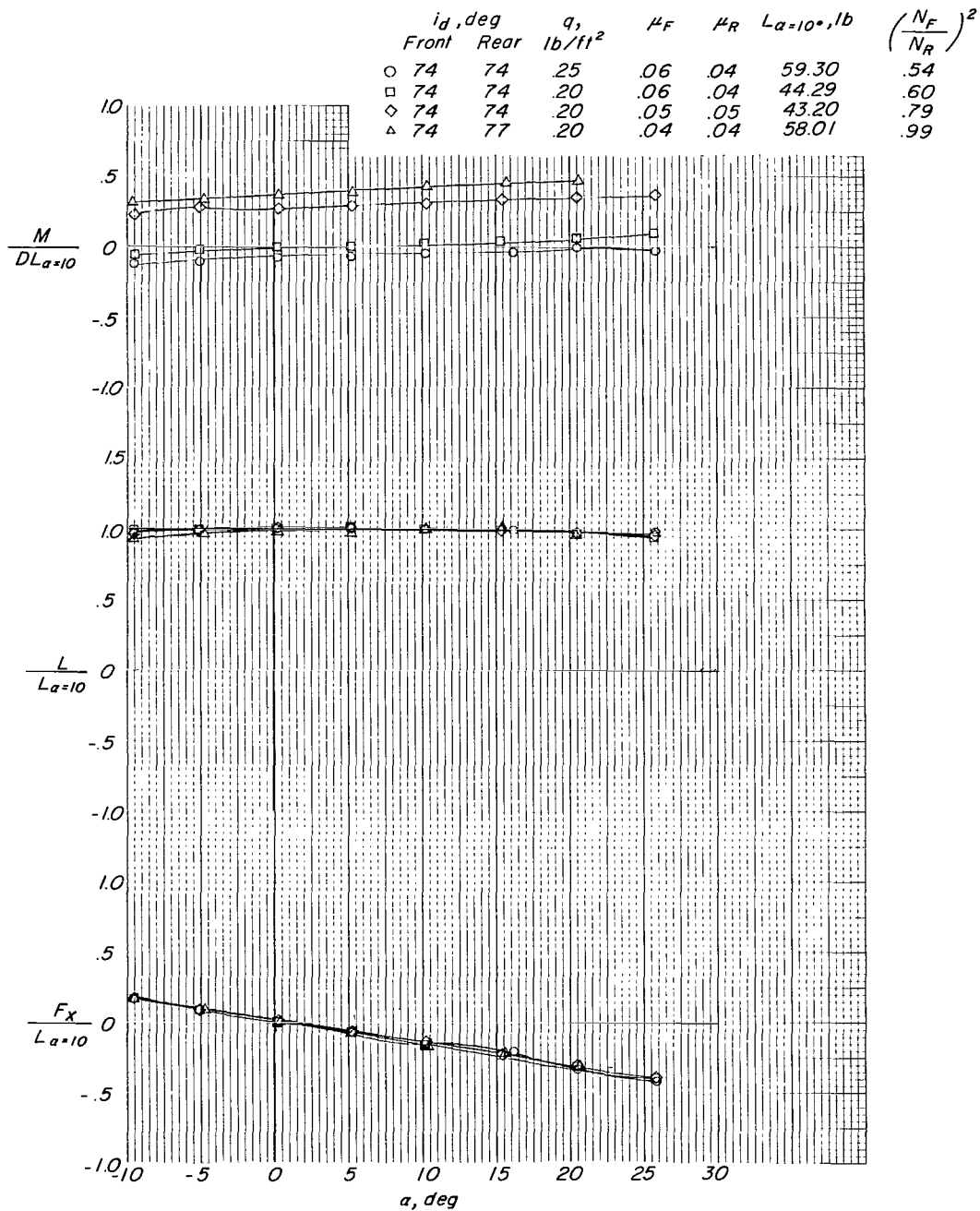
(a) Complete model.

Figure 12.- Aerodynamic characteristics with differential thrust. $i_d \approx 75°$.

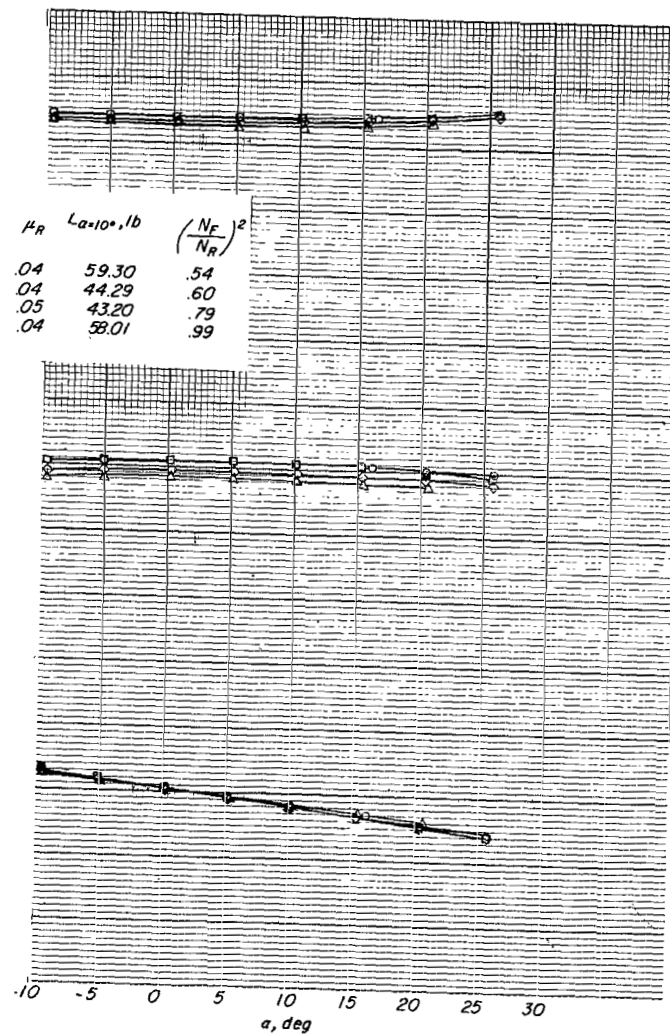|	i_d, deg		q,	μ_F	μ_R	$L_{a=10^\circ}$, lb	$\left(\dfrac{N_F}{N_R}\right)^2$
	Front	Rear	lb /ft²				
○	74	74	.25	.06	.04	59.30	.54
□	74	74	.20	.06	.04	44.29	.60
◇	74	74	.20	.05	.05	43.20	.79
△	74	77	.20	.04	.04	58.01	.99

(b) Front ducts.

(c) Rear ducts.

Figure 12.- Concluded.

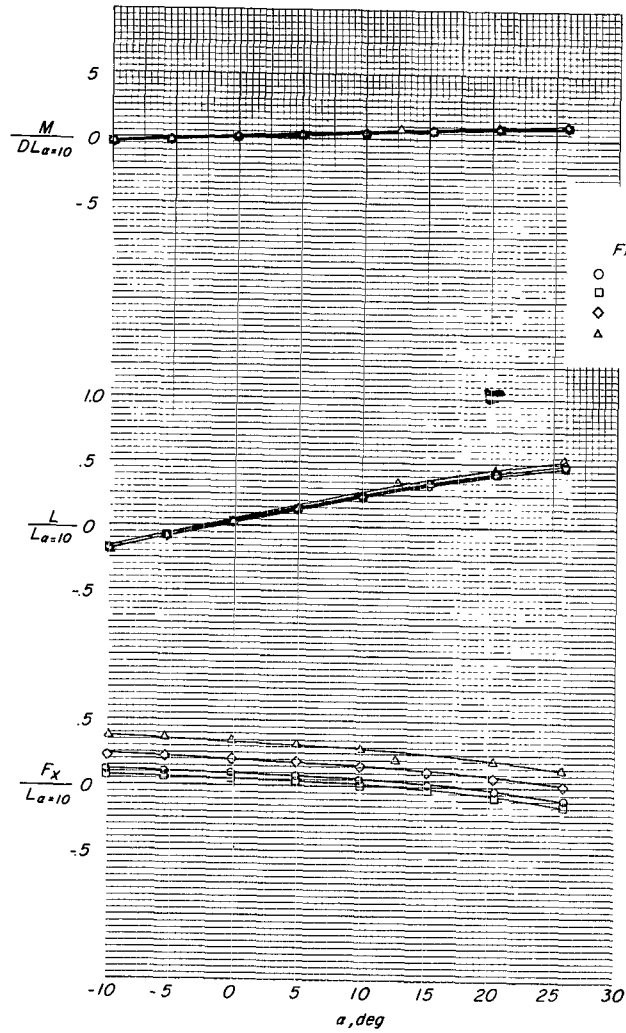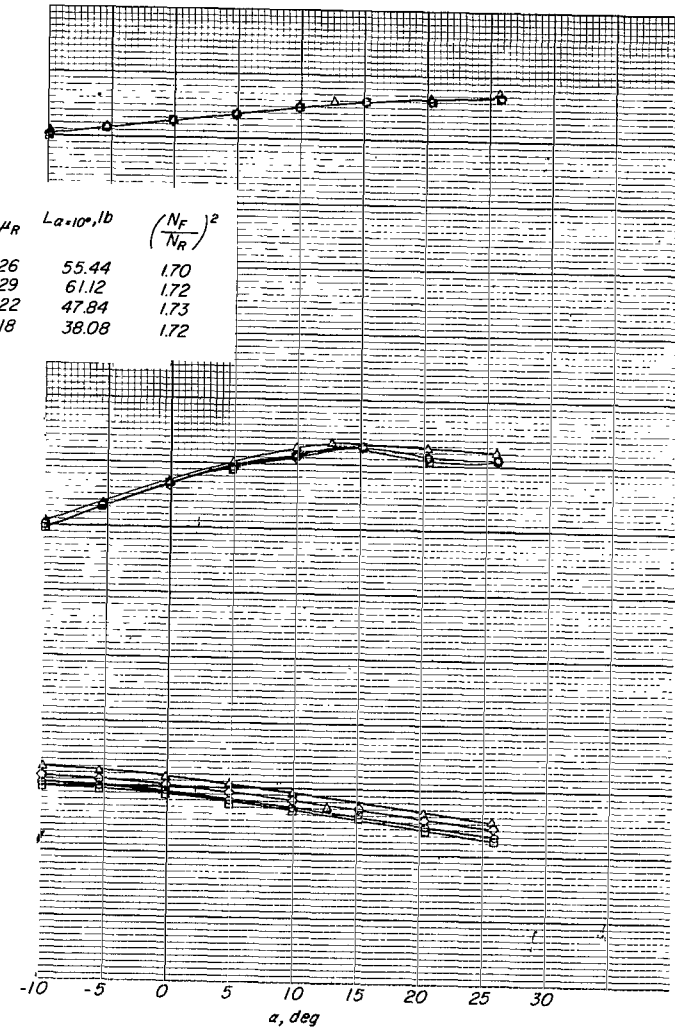|	i_d, deg		q,	μ_F	μ_R	$L_{a=10°}$, lb	$\left(\dfrac{N_F}{N_R}\right)^2$
	Front	Rear	lb /ft²				
○	0	17	4.23	.20	.26	55.44	1.70
□	0	17	5.08	.22	.29	61.12	1.72
◇	0	17	2.96	.17	.22	47.84	1.73
△	0	17	1.99	.14	.18	38.08	1.72
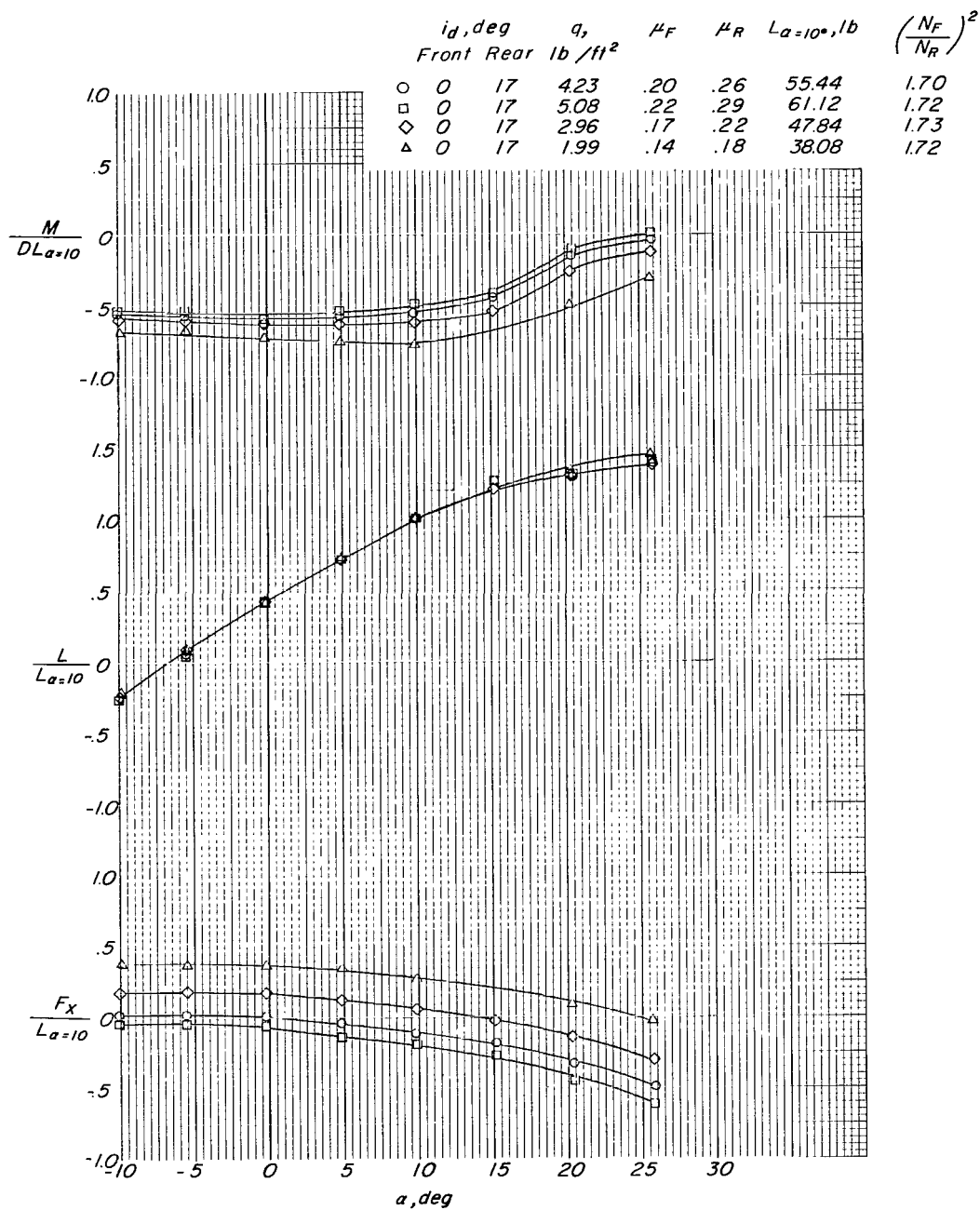
(a) Complete model.

Figure 13.- Aerodynamic characteristics during acceleration and deceleration. $i_{d,F} = 0°$; $i_{d,R} = 17°$.

$\dfrac{M}{DL_{a=10}}$
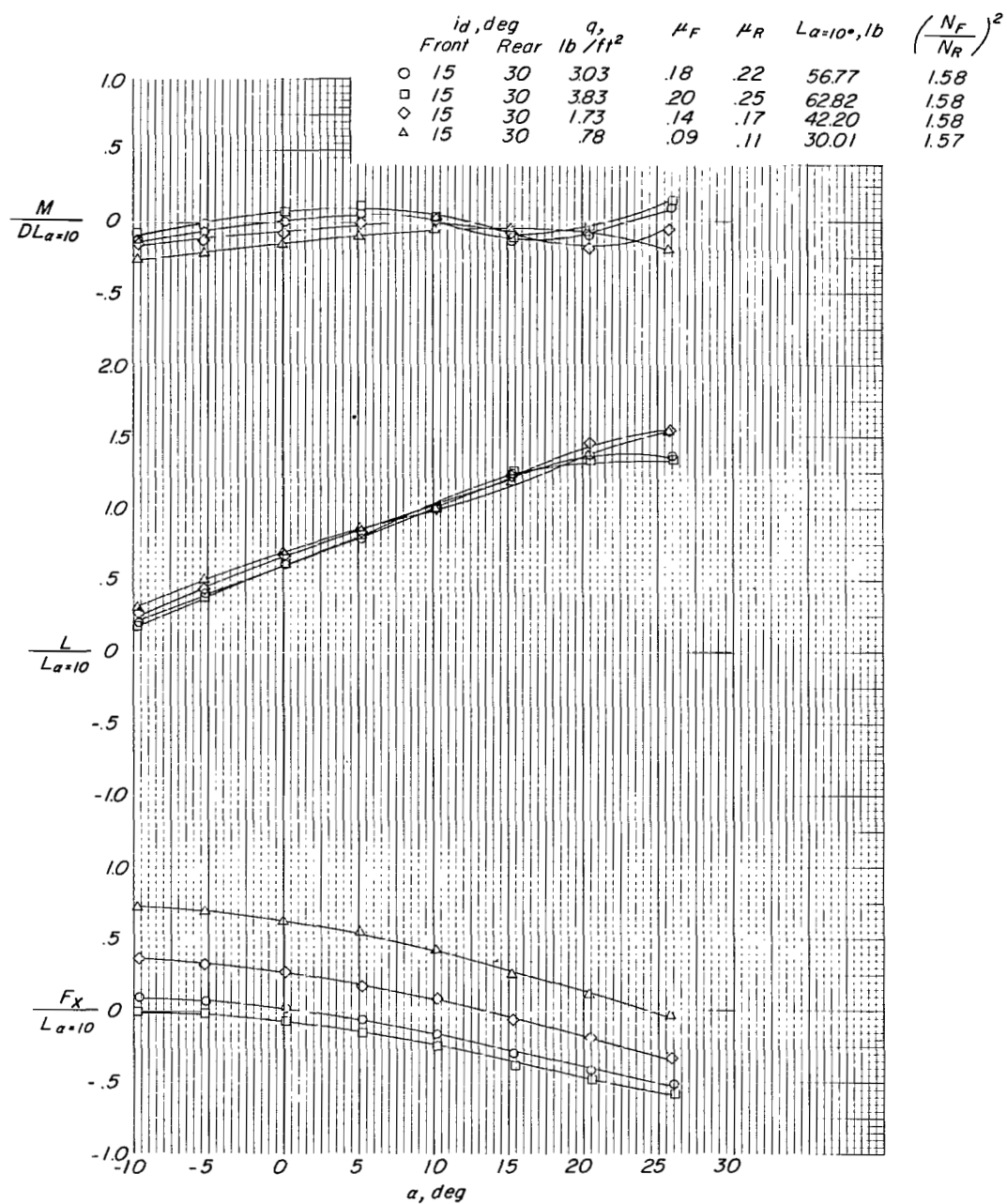
$\dfrac{L}{L_{a=10}}$

$\dfrac{F_x}{L_{a=10}}$

	i_d, deg		q,	μ_F	μ_R	$L_{a=10}$, lb	$\left(\dfrac{N_F}{N_R}\right)^2$
	Front	Rear	lb/ft²				
○	0	17	4.23	.20	.26	55.44	1.70
□	0	17	5.08	.22	.29	61.12	1.72
◇	0	17	2.96	.17	.22	47.84	1.73
△	0	17	1.99	.14	.18	38.08	1.72

a, deg

a, deg

(b) Front ducts.

(c) Rear ducts.

Figure 13.- Concluded.

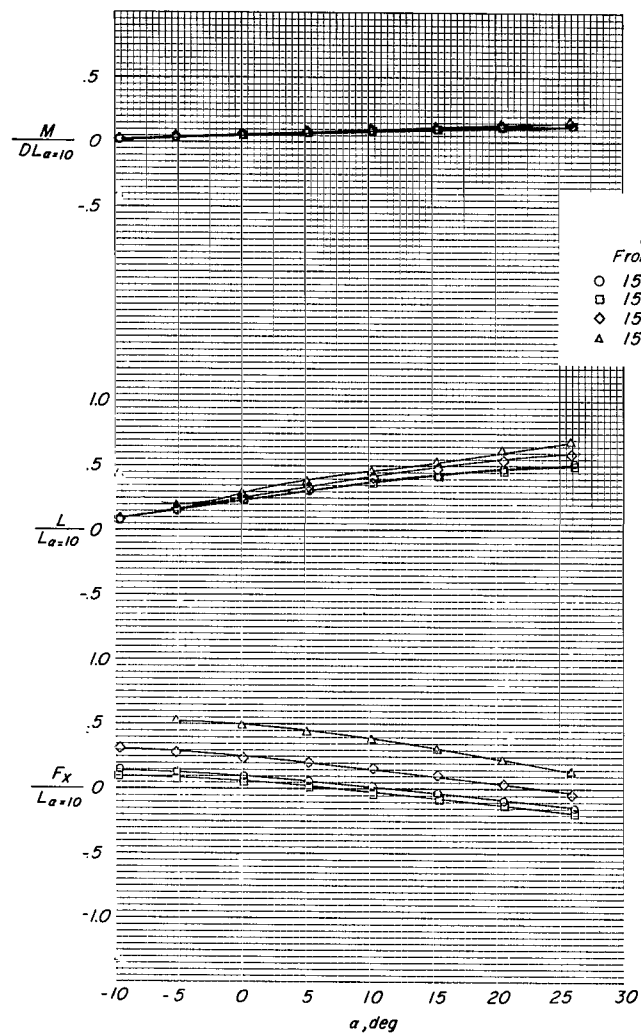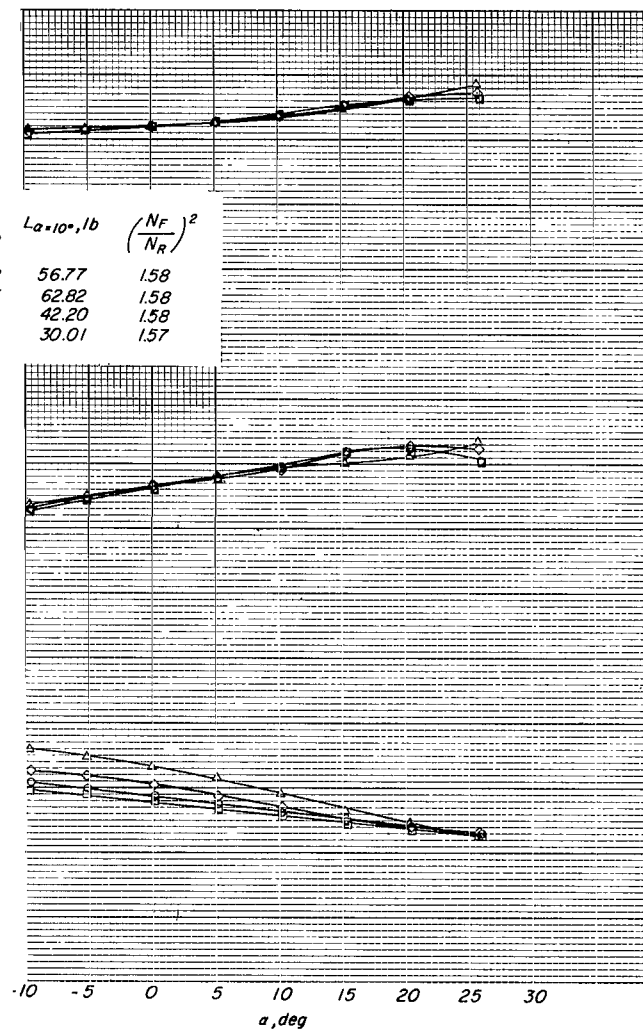|	i_d, deg		q,	μ_F	μ_R	$L_{a=10°}$, lb	$\left(\dfrac{N_F}{N_R}\right)^2$
	Front	Rear	lb /ft²				
○	15	30	3.03	.18	.22	56.77	1.58
□	15	30	3.83	.20	.25	62.82	1.58
◇	15	30	1.73	.14	.17	42.20	1.58
△	15	30	.78	.09	.11	30.01	1.57

(a) Complete model.

Figure 14.- Aerodynamic characteristics during acceleration and deceleration. $i_{d,F} = 15°$; $i_{d,R} = 30°$.

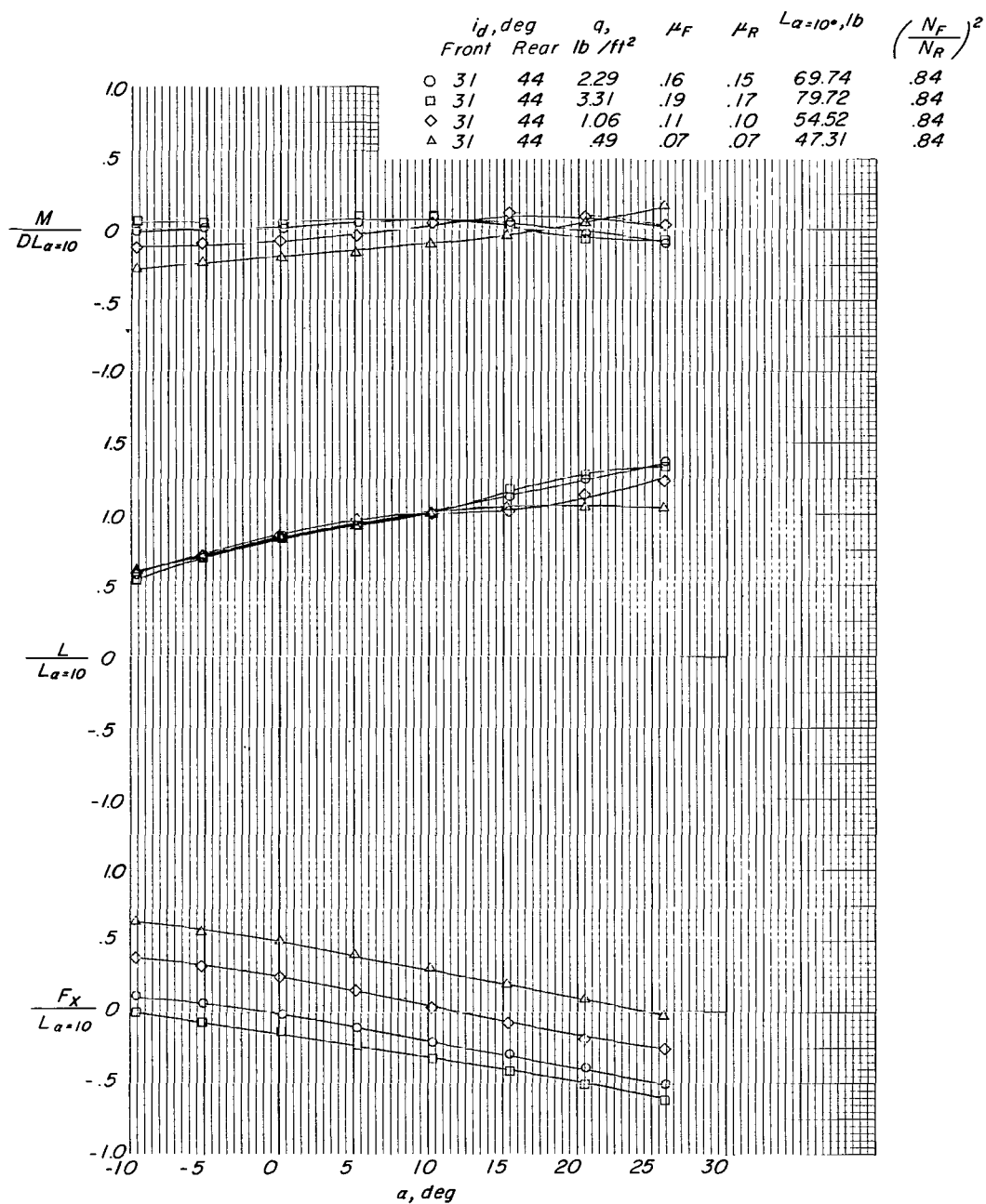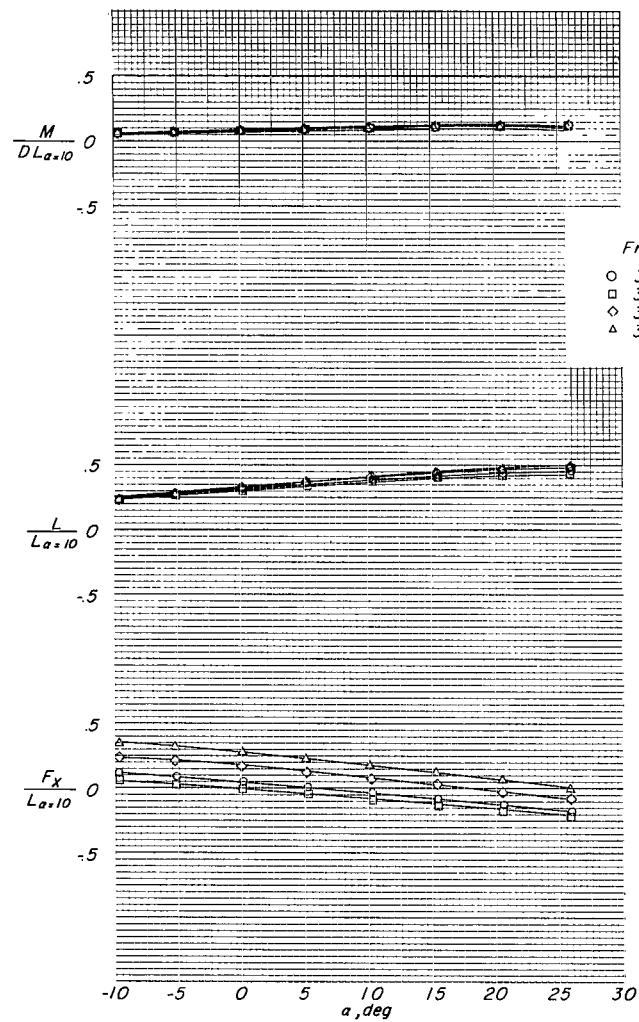|	i_d, deg		q,	μ_F	μ_R	$L_{a=10^\circ}$, lb	$\left(\dfrac{N_F}{N_R}\right)^2$
	Front	Rear	lb /ft²				
○	15	30	3.03	.18	.22	56.77	1.58
□	15	30	3.83	.20	.25	62.82	1.58
◇	15	30	1.73	.14	.17	42.20	1.58
△	15	30	.78	.09	.11	30.01	1.57

(b) Front ducts.

(c) Rear ducts.

Figure 14.- Concluded.
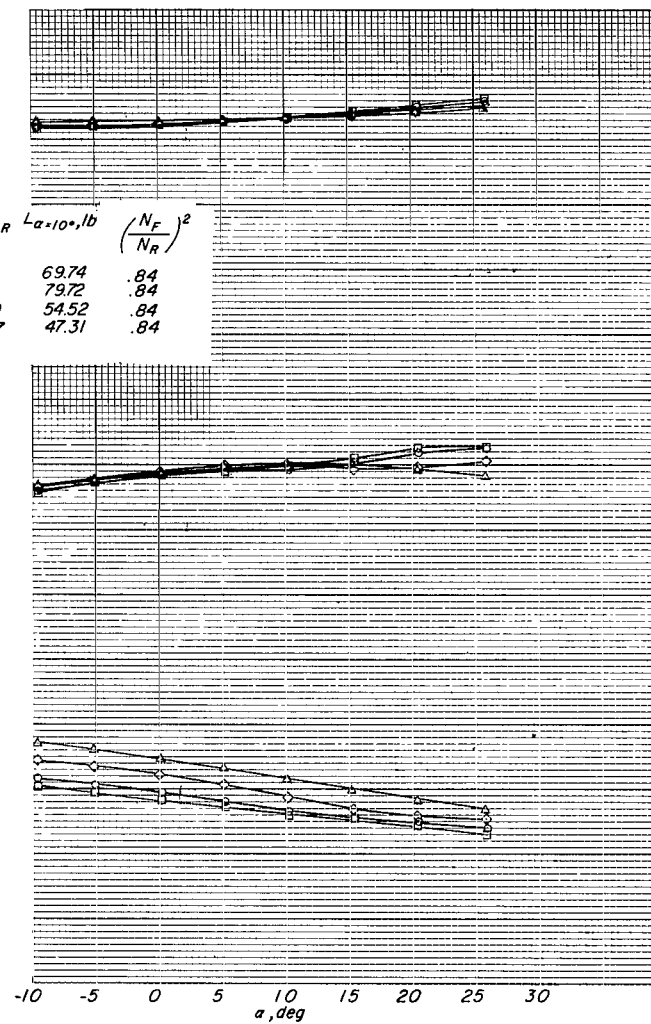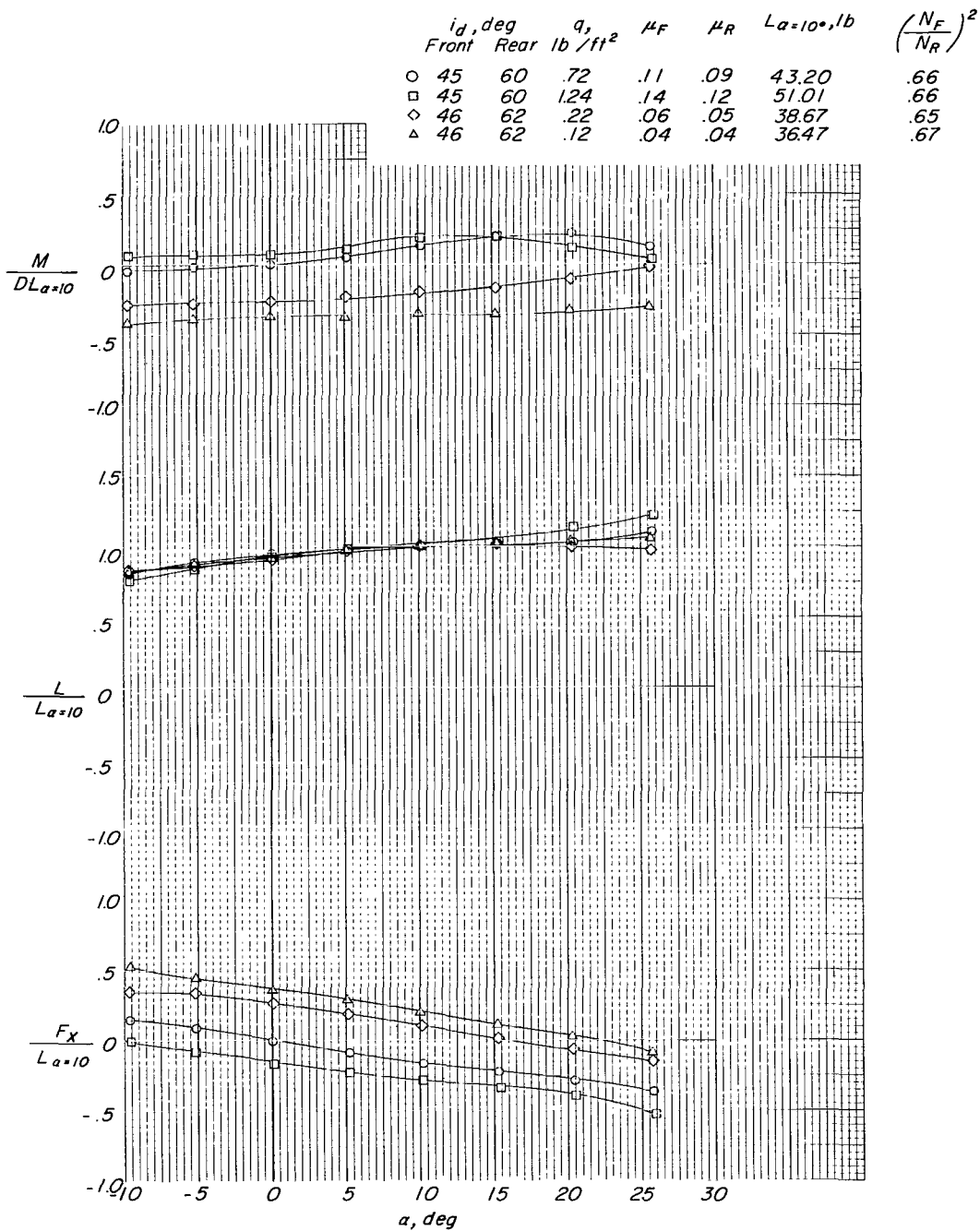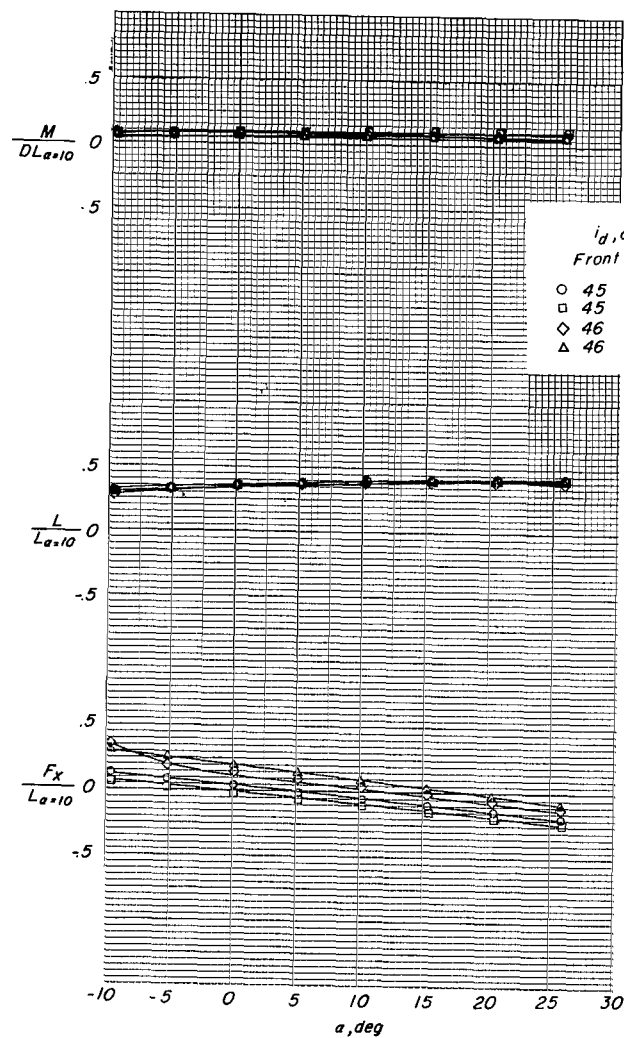
(a) Complete model.

Figure 15.- Aerodynamic characteristics during acceleration and deceleration. $i_{d,F} = 31°$; $i_{d,R} = 44°$.

	i_d, deg		q,	μ_F	μ_R	$L_{a=10°}$, lb	$\left(\dfrac{N_F}{N_R}\right)^2$
	Front	Rear	lb/ft²				
○	31	44	2.29	.16	.15	69.74	.84
□	31	44	3.31	.19	.17	79.72	.84
◇	31	44	1.06	.11	.10	54.52	.84
△	31	44	.49	.07	.07	47.31	.84

(b) Front ducts.　　　　　(c) Rear ducts.

Figure 15.- Concluded.

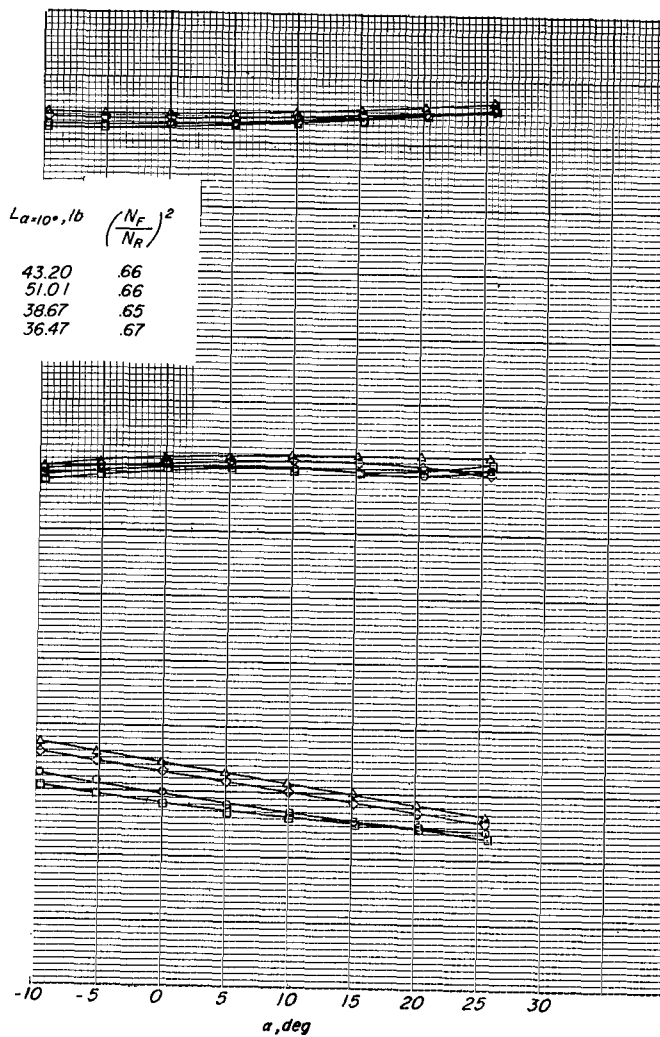|	i_d, deg		q,	μ_F	μ_R	$L_{a=10°}$, lb	$\left(\dfrac{N_F}{N_R}\right)^2$
	Front	Rear	lb/ft^2				
○	45	60	.72	.11	.09	43.20	.66
□	45	60	1.24	.14	.12	51.01	.66
◇	46	62	.22	.06	.05	38.67	.65
△	46	62	.12	.04	.04	36.47	.67

(a) Complete model.

Figure 16.- Aerodynamic characteristics during acceleration and deceleration. $i_{d,F} \approx 45°$; $i_{d,R} \approx 60°$.

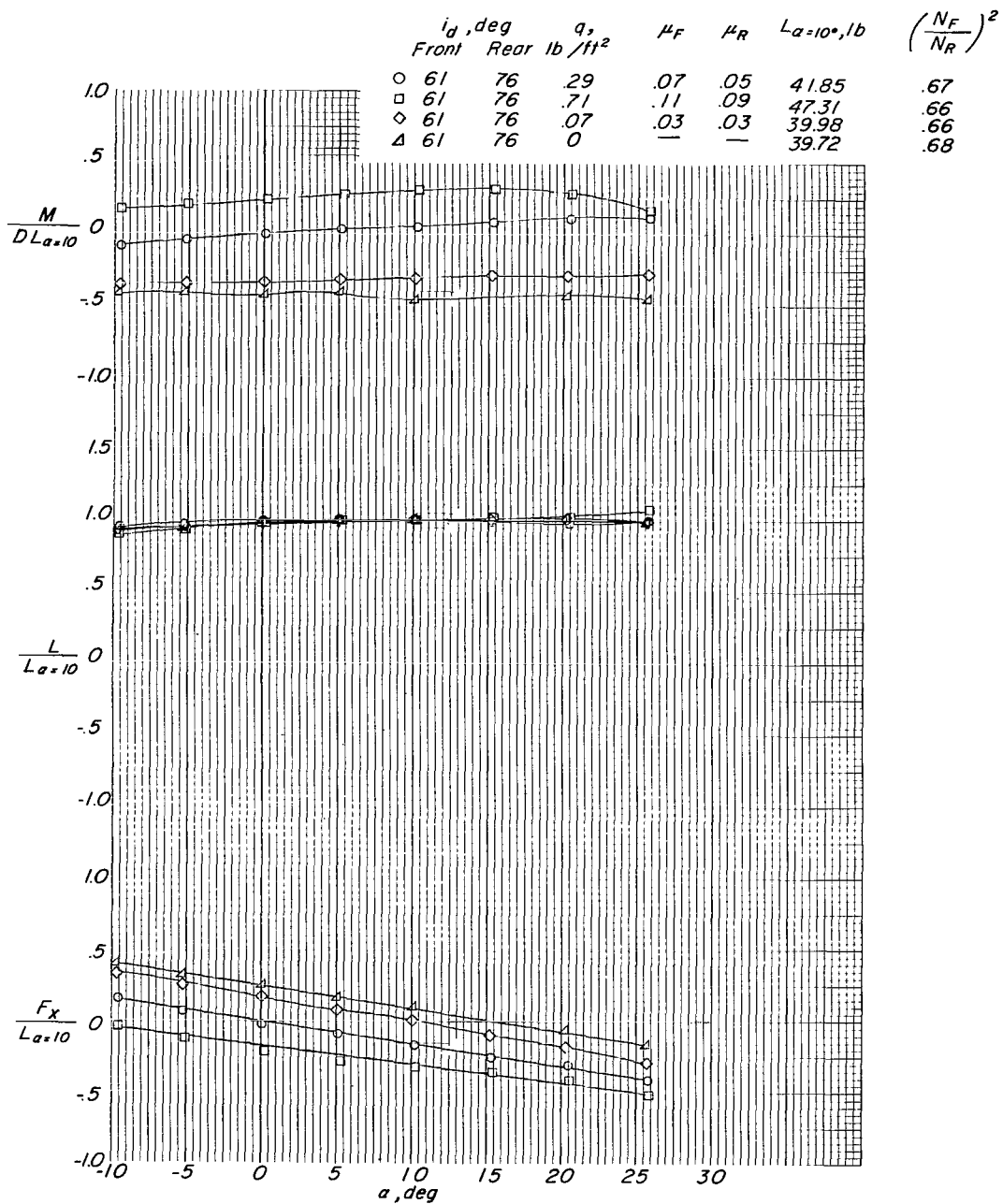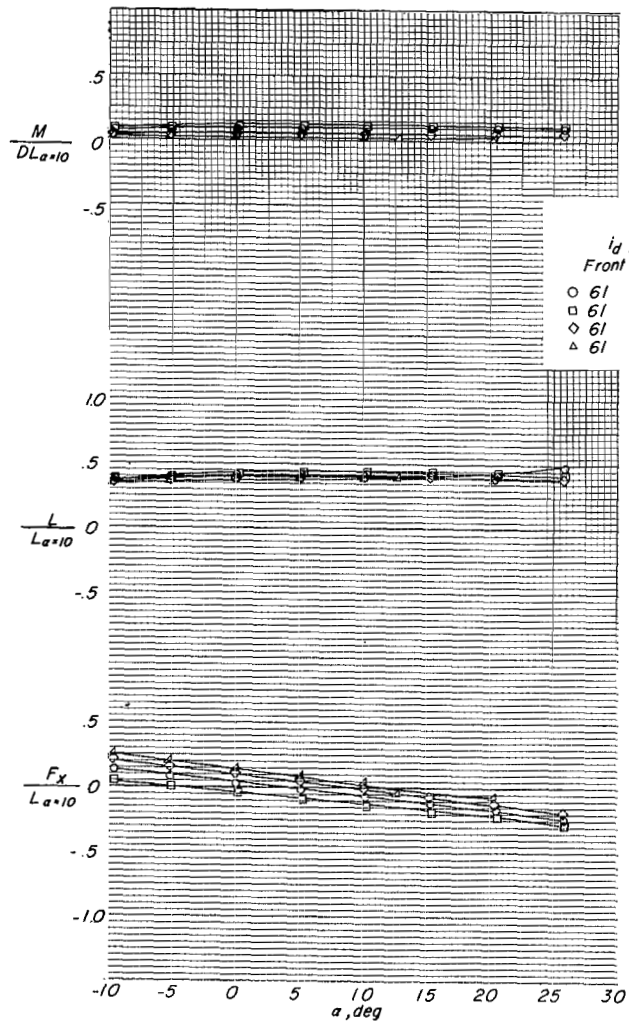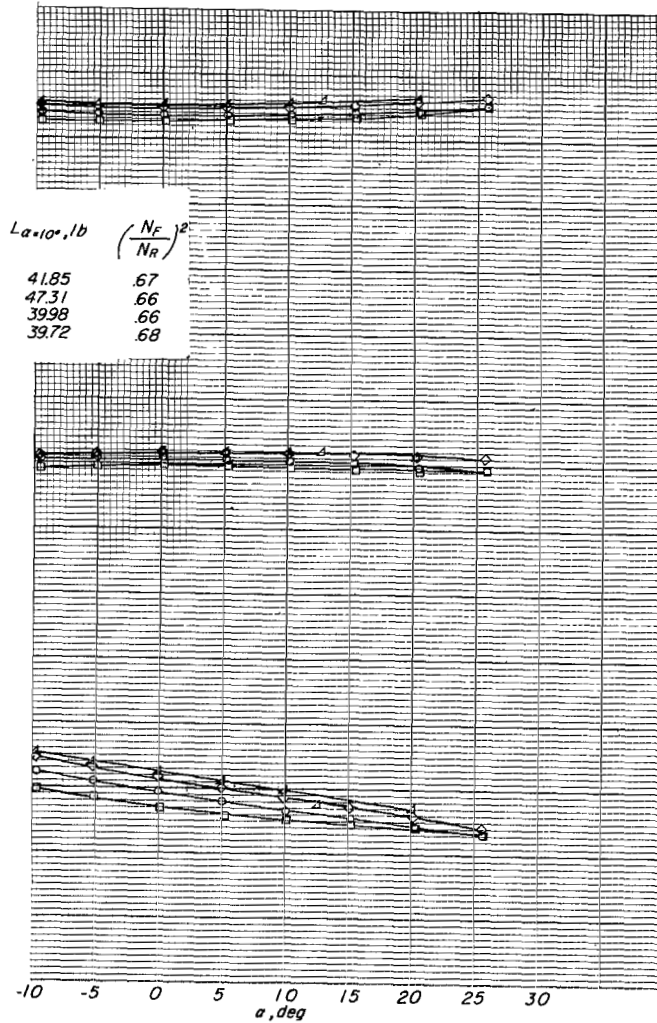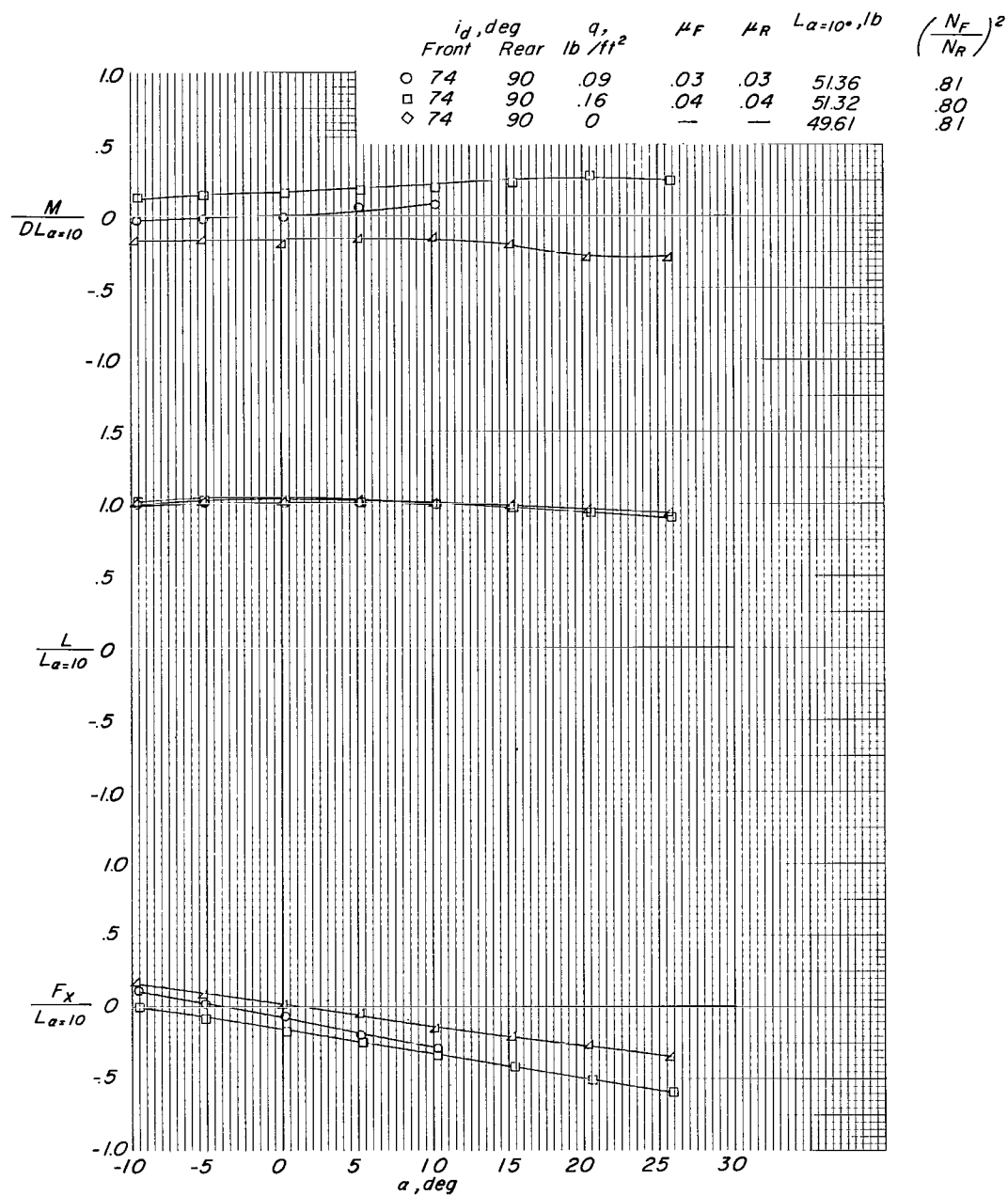|	i_d, deg		q,	μ_F	μ_R	$L_{a=10°}$, lb	$\left(\dfrac{N_F}{N_R}\right)^2$
	Front	Rear	lb/ft²				
○	45	60	.72	.11	.09	43.20	.66
□	45	60	1.24	.14	.12	51.01	.66
◇	46	62	.22	.06	.05	38.67	.65
△	46	62	.12	.04	.04	36.47	.67

(b) Front ducts.

(c) Rear ducts.

Figure 16.- Concluded.

	i_d, deg		q,	μ_F	μ_R	$L_{a=10°}$, lb	$\left(\dfrac{N_F}{N_R}\right)^2$
	Front	Rear	lb /ft²				
○	61	76	.29	.07	.05	41.85	.67
□	61	76	.71	.11	.09	47.31	.66
◇	61	76	.07	.03	.03	39.98	.66
△	61	76	0	—	—	39.72	.68

$$\frac{M}{DL_{a=10}}$$

$$\frac{L}{L_{a=10}}$$

$$\frac{F_x}{L_{a=10}}$$

a, deg

(a) Complete model.

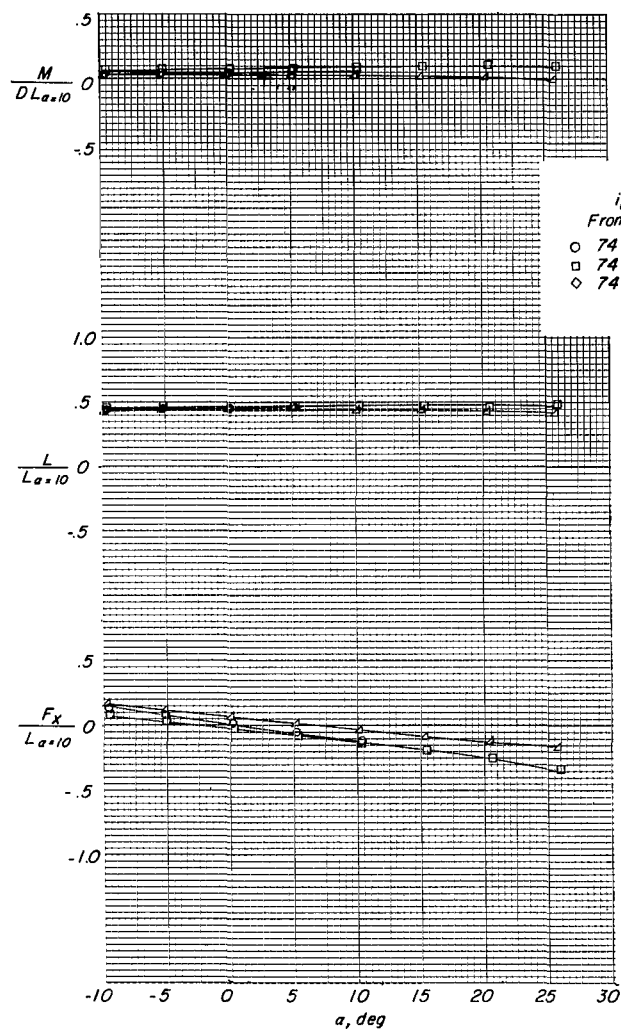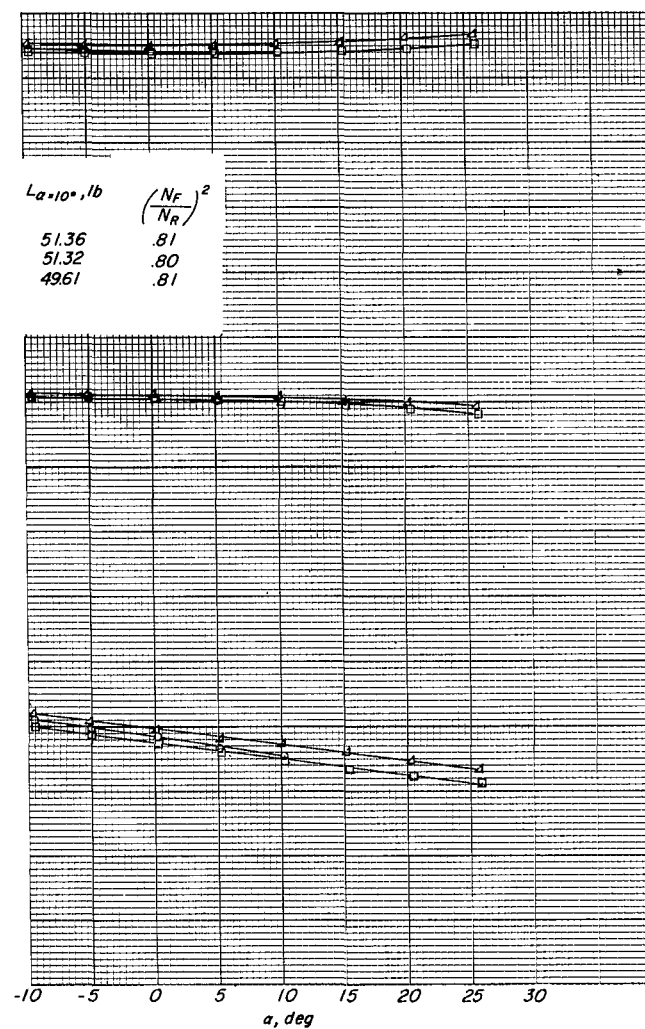Figure 17.- Aerodynamic characteristics during acceleration and deceleration. $i_{d,F} = 61°$; $i_{d,R} = 76°$.

47

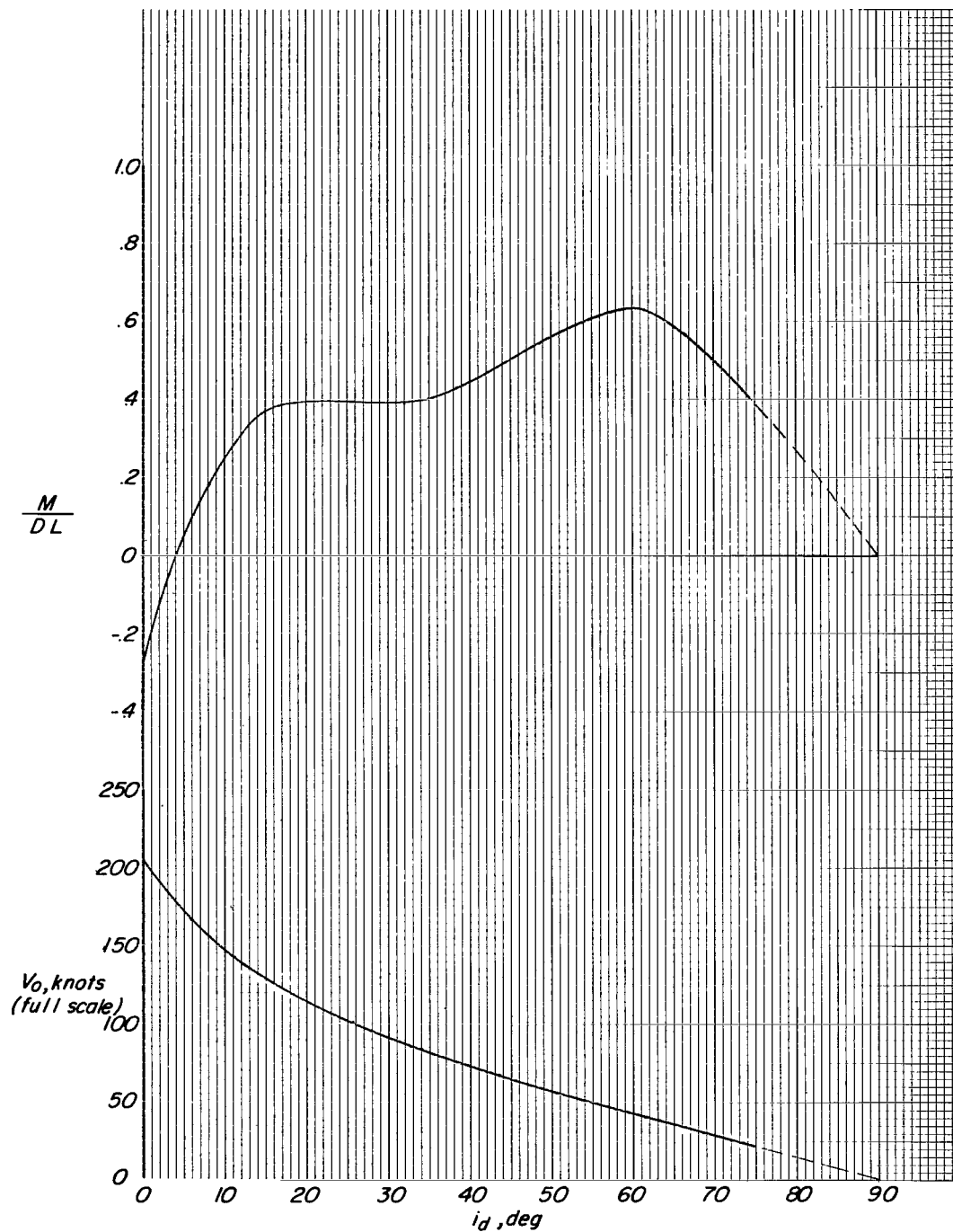|	i_d, deg		q,	μ_F	μ_R	$L_{a=10°}$, lb	$\left(\dfrac{N_F}{N_R}\right)^2$
	Front	Rear	lb/ft²				
○	61	76	.29	.07	.05	41.85	.67
□	61	76	.71	.11	.09	47.31	.66
◇	61	76	.07	.03	.03	39.98	.66
△	61	76	0	—	—	39.72	.68

(b) Front ducts.

(c) Rear ducts.

Figure 17.- Concluded.

(a) Complete model.

Figure 18.- Aerodynamic characteristics during acceleration and deceleration. $i_{d,F} = 74^\circ$; $i_{d,R} = 90^\circ$.
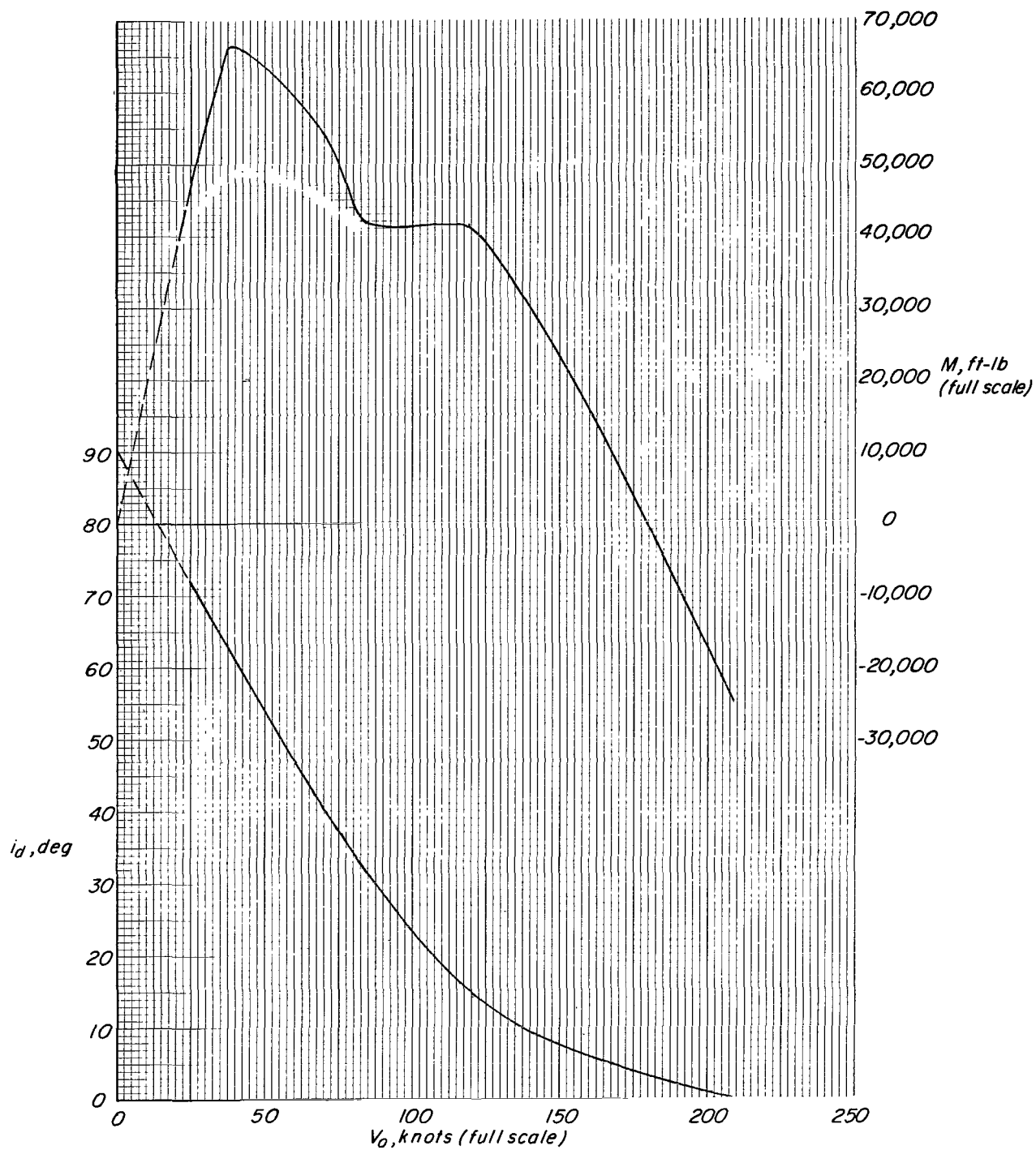
	i_d, deg		q,	μ_F	μ_R	$L_{a=10°}$, lb	$\left(\dfrac{N_F}{N_R}\right)^2$
	Front	Rear	lb/ft²				
○	74	90	.09	.03	.03	51.36	.81
□	74	90	16	.04	04	51.32	.80
◇	74	90	0	—	—	49.61	.81

(b) Front ducts.

(c) Rear ducts.

Figure 18.- Concluded.

(a) Variation of M/DL and V_O with i_d.

Figure 19.- Transitional characteristics of basic configuration. $i_{d,F} = i_{d,R}$; $N_F = N_R$; $(\alpha)_{F_X=0} = 0$.

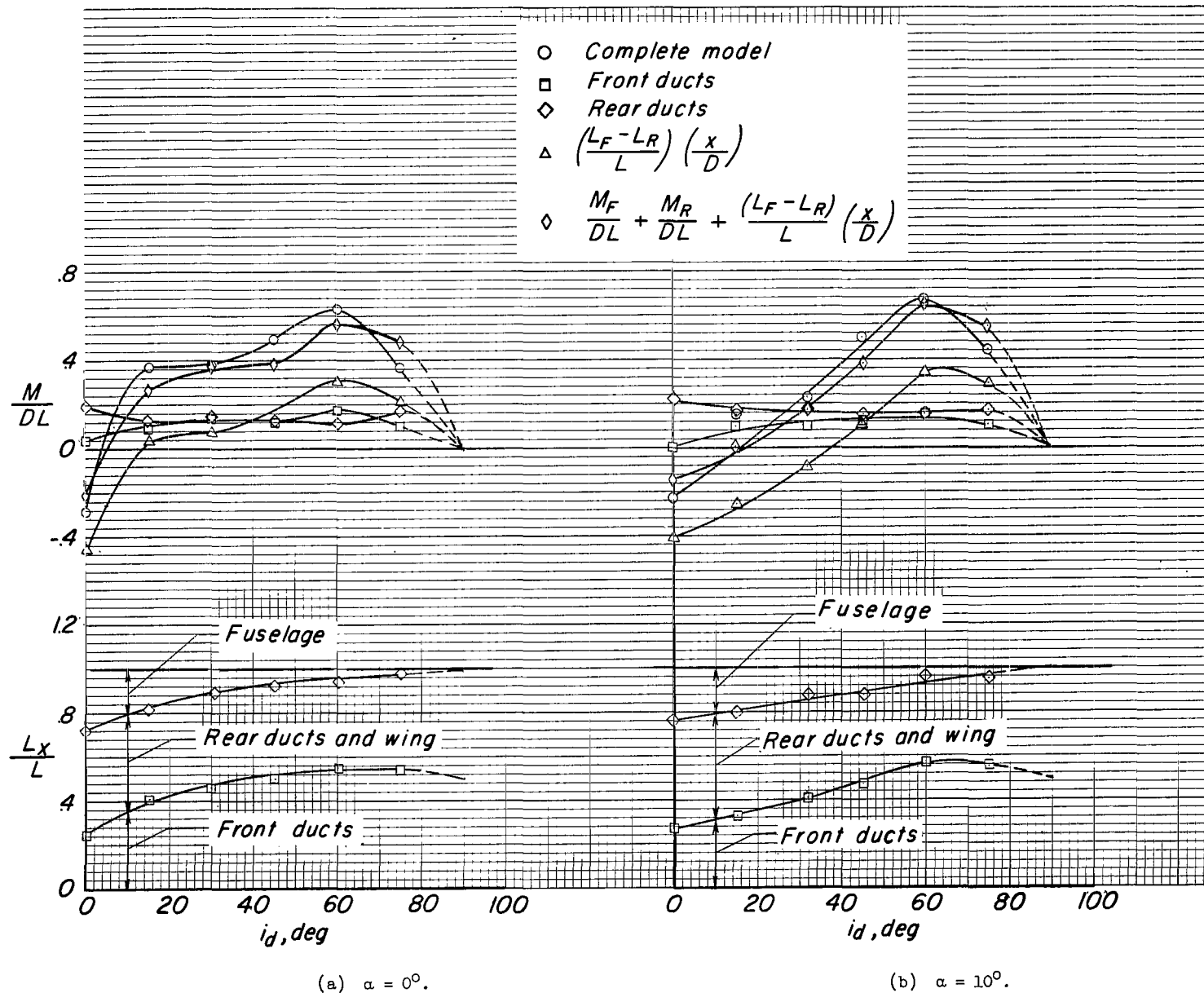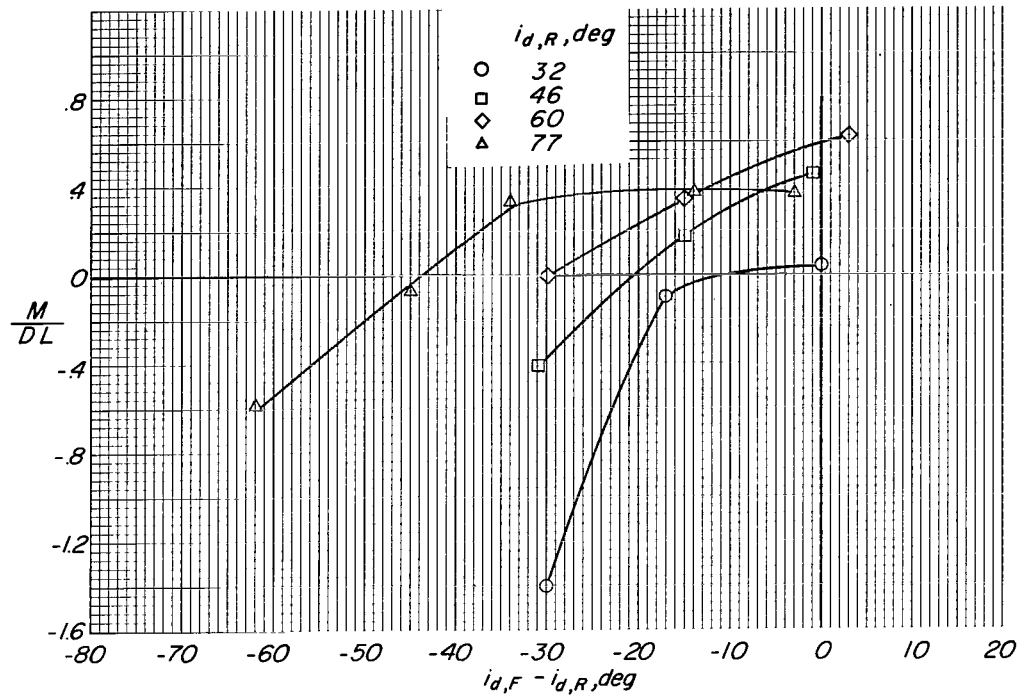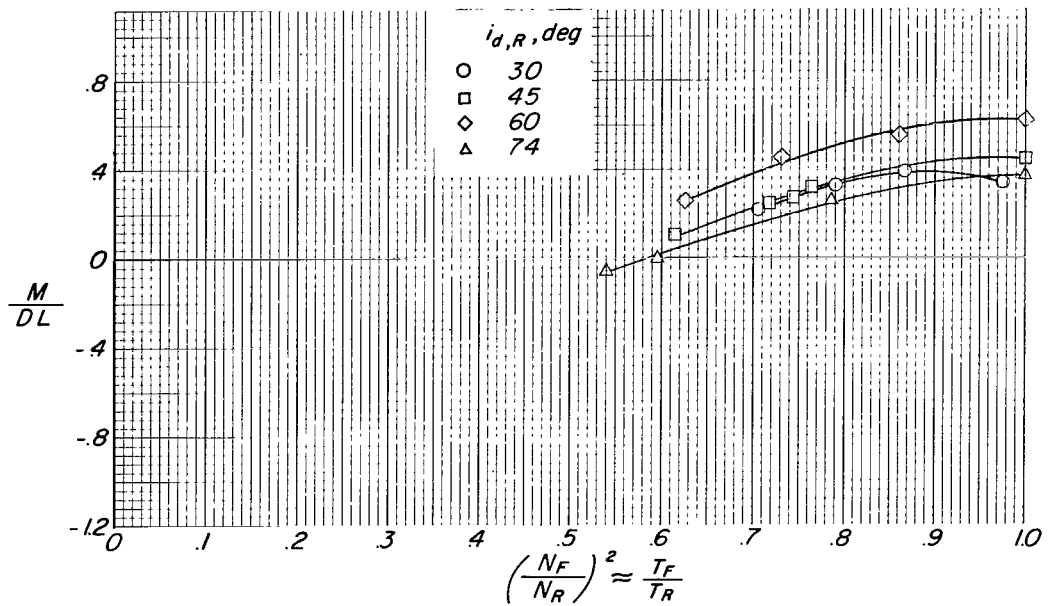(b) Variation of moment and incidence (full scale) with velocity.

Figure 19.- Concluded.

Figure 20.- Lift and pitching-moment characteristics of basic configuration. $i_{d,F} = i_{d,R}$; $N_F \approx N_R = 0$.

(a) Effects of differential duct incidence. $\frac{T_F}{T_R} \approx 1.00$.

(b) Effects of differential thrust. $i_{d,F} = i_{d,R}$.

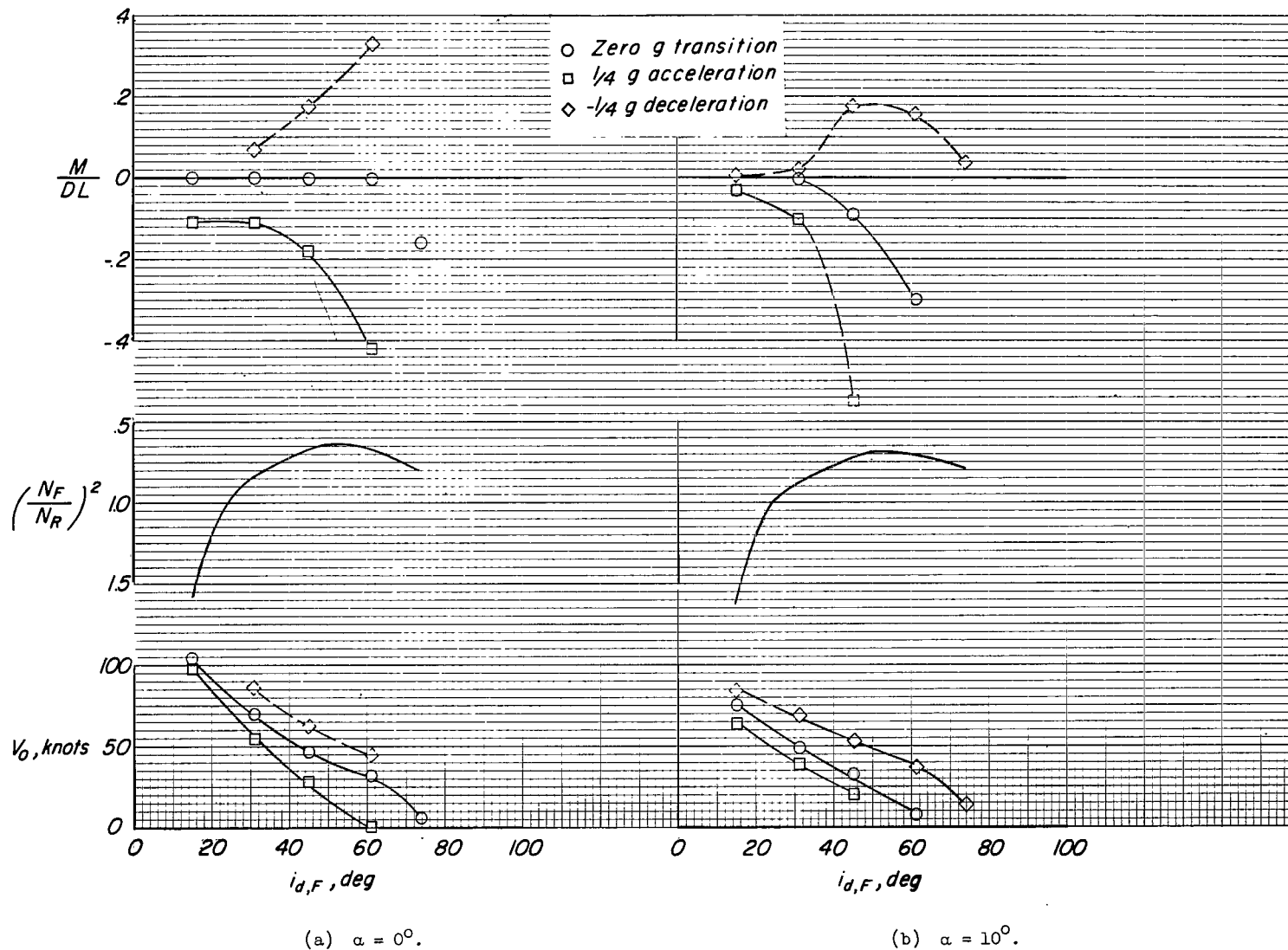Figure 21.- Effect of varying thrust and duct incidence on pitching moment. $\alpha = 0^\circ$.

(a) α = 0°.

(b) α = 10°.

Figure 22.- Transitional characteristics at α = 0° and α = 10°. $i_{d,R} \approx i_{d,F} + 15°$.

NASA SCIENTIFIC AND TECHNICAL PUBLICATIONS

TECHNICAL REPORTS: Scientific and technical information considered important, complete, and a lasting contribution to existing knowledge.

TECHNICAL NOTES: Information less broad in scope but nevertheless of importance as a contribution to existing knowledge.

TECHNICAL MEMORANDUMS: Information receiving limited distribution because of preliminary data, security classification, or other reasons.

CONTRACTOR REPORTS: Technical information generated in connection with a NASA contract or grant and released under NASA auspices.

TECHNICAL TRANSLATIONS: Information published in a foreign language considered to merit NASA distribution in English.

TECHNICAL REPRINTS: Information derived from NASA activities and initially published in the form of journal articles or meeting papers.

SPECIAL PUBLICATIONS: Information derived from or of value to NASA activities but not necessarily reporting the results of individual NASA-programmed scientific efforts. Publications include conference proceedings, monographs, data compilations, handbooks, sourcebooks, and special bibliographies.

Details on the availability of these publications may be obtained from:

SCIENTIFIC AND TECHNICAL INFORMATION DIVISION

NATIONAL AERONAUTICS AND SPACE ADMINISTRATION

Washington, D.C. 20546